Results in Physics 22 (2021) 103962

Contents lists available at ScienceDirect

Results in Physics

journal homepage: www.elsevier.com/locate/rinp

Effects of materials positioning and tool rotational speed on metallurgical and mechanical properties of dissimilar modified friction stir clinching of AA5754-O and AA2024-T3 sheets

S. Memon [a], M. Paidar [b,*], S. Mehrez [c], K. Cooke [d,*], O.O. Ojo [e], H.M. Lankarani [a]

[a] Department of Mechanical Engineering, Wichita State University, Wichita, United States
[b] Department of Material Engineering, South Tehran Branch, Islamic Azad University, Tehran 1459853849, Iran
[c] Department of Mechanical Engineering, College of Engineering at Al Kharj, Prince Sattam bin Abdulaziz University, 16273, Saudi Arabia
[d] Faculty of Engineering and Informatics, University of Bradford, Richmond Road, BD7 1DP Bradford, West Yorkshire, UK
[e] Department of Industrial and Production Engineering, The Federal University of Technology Akure, Nigeria

ARTICLE INFO

Keywords:
Modified friction stir clinching
Friction stir spot welding
Aluminium alloys
Material positioning
Microstructure
Mechanical properties
Fracture

ABSTRACT

The performance of the modified friction stir clinched and friction stir spot welded joints of AA5754-O and AA2024-T3 Al alloy was improved by investigating the impact of material flow influencing parameters such as material positioning and tool rotational speed on the microstructure, mechanical and fracture behaviors of the joints. The results reveal that the positioning of a harder material (AA2024-T3) as the upper plate induces higher peak temperatures in the friction stir clinched (500 °C) and friction stir spot welded (475 °C) joints. This positioning favors inter-material mingling, grain coarsening with inherent higher dislocation density and tangles, and improved tensile failure loads in the AA2024-T3/AA5754-O joint than the AA5754-O/AA2024-T3 joint. The formation of partial weld-center defect declines in the AA2024-T3/AA5754-O at low tool rotational speed due to the better local heat build-up and geometric-differential flow effect in comparison with the AA5754-O/AA2024-T3 counterparts. The positioning of harder Al alloy on the top of a soft Al alloy is thus recommended for the improvement of modified friction stir clinched joints.

Introduction

Literature assessment indicates that material flow influencing parameters, such as tool design, process parameters, process modification, and material positioning, are critical for the overall integrity/performance of friction stir welds, friction stir lap welds, friction stir spot welds [1–7] and other friction-based manufacturing processes [8–11]. The required metallurgical bonding of joints is dependent on the material flow and intermingling level. The studies of Dialami et al. [12] revealed that abnormal flow/stirring and undesirable heat input, either excessive or insufficient, are responsible for improper bonding, inter-material flow, and weld discontinuities/defects such as cavities, voids, flash, and wormhole. Higher levels of tool rotational speed are directly related to heat input and flowability of the plasticized materials during the friction stir welding of AA7075 Al alloy in the works of Rouzbehani et al. [13]. Shah et al. [14] reported that an increase in the tool eccentricity enhanced the induced inter-material mixing and further aided grain refinement in the inner band zone and the formation of high-density platelet-like precipitates in the friction stir welded AA6061 Al alloy. Thus, there is a need to further improve the performance of the newly developed friction stir based welding methods via the assessment of material flow influencing parameters such as material positioning.

The role of material positioning on material flow and inter-mixing has been investigated via the use of friction stir welding (FSW), friction stir lap welding (FSLP), and friction stir spot welding processes. The positioning of softer Al alloy at the advancing side has been reported to favor better material flow for increased weld performance. For instance, the investigation of Mabuwa and Msomi [15] showed that the positioning of AA1050-H14 on the advancing side during the joining of AA1050-H14 and AA6082-T6 Al alloys enhanced the tensile strength (83 MPa), percentage elongation (22.1%), yield strength (61 MPa), and hardness (80 HV). A higher force acts on the plates when a higher strength material (AA2024 Al alloy) is placed/positioned on the advancing side in the studies of Cavaliere et al. [16]. The best fatigue

* Corresponding authors.
E-mail addresses: m.paidar@srbiau.ac.ir (M. Paidar), k.cooke1@bradford.ac.uk (K. Cooke).

https://doi.org/10.1016/j.rinp.2021.103962
Received 28 November 2020; Received in revised form 5 February 2021; Accepted 6 February 2021
Available online 11 February 2021
2211-3797/© 2021 The Authors. Published by Elsevier B.V. This is an open access article under the CC BY license (http://creativecommons.org/licenses/by/4.0/).

Table 1
Chemical composition of base alloys (wt.%).

Si	Mn	Fe	Cr	Cu	Mg	Al	Alloy
0.08	0.62	0.44	0.012	4.90	1.28	Base	AA2024-T3
0.61	0.03	0.26	0.037	0.02	3.17	Base	AA5754-O

Table 2
Mechanical properties of the base alloys.

Elongation (%)	Yield Strength [MPa]	Ultimate Tensile Strength [MPa]	Alloy
14	317	448	AA2024-T3
15	196	217	AA5754-O

behavior was obtained in the AA6082-AA2024 joint (AA6082 at the advancing side) while inherent forging defect caused fracture initiation in the AA2024-AA6082 joint (AA2024 at the advancing side) [16]. Pabandi et al. [17] reported that adequate plastic material inter-mixing and improved tensile strength ensued when AA6061-T6 Al alloy was positioned at the advancing side during the friction stir welding of AA2024-T6 and AA6061-T6 Al alloys. According to Paidar et al. [18], improved strength was also obtained in the AA2024-T3/AA6061-T6 joint when compared to the AA6061-T6/AA2024-T3 joint. Jeon et al. [19] reported that material position was not a dominant fracture influencing parameter in the friction stir spot welded 5052-H32/6061-T6 joints but hook defect was a major stress raiser irrespective of the position of Al alloys.

According to Paidar et al. [20], the modified friction stir clinching (MFSC) is a variance of the conventional friction stir clinching (FSC) process where a 2-step approach is utilized to eliminate both the inherent keyhole and bulk protrusion of the FSC process. Paidar et al. [21] investigated the MFSC of the AA2024-T3/AA7075-T6 aluminum alloys. The MFSC process improved the bond/shear area, caused the formation of geometric-differential flow defect and atomic diffusion-induced Mg_2Si and Al_2CuMg phases. Improved strengths of about 83% (tensile shear) and 50% (cross tensile) have been achieved in the MFSC welded AA2024-T3/AA6061-T6 joints as compared to the conventional friction stir spot welded joints in the studies of Paidar et al. [22]. The weldability [19–20], self-reacting brazing [23,24], precipitation-hardening heat treatment [25] of MFSC joints have been studied. The impacts of process parameters such as stirring time [26] and penetration depth [20] on the MFSC joint have also been examined. However, the elucidation of the flow-influencing parameters (such as material positioning, tool design, and process conditions) in dissimilar MFSC welds to improve weld performance is an important research area having a paucity of information in the literature.

Thus, this paper elucidates the combined effect of material positioning and tool rotational speed on the recently developed modified friction stir clinching (MFSC) of AA5754-O and AA2024-T3 alloys towards achieving an improved weld strength. The material flow pattern associated with material positioning, microstructure, mechanical properties, and fracture behaviors of the modified friction stir clinched AA5754-O and AA2024-T3 joints were studied and compared with those of the friction stir spot welded (FSSW) joints.

Experimental procedure

The base materials employed for this research are 1.6 mm thick AA2024-T3 and 1.5 mm thick AA5754-O Al alloys (supplied by Hezar Aluminum, Iran). The chemical compositions and mechanical properties of the base alloys are provided in Tables 1 and 2 respectively. The as-received alloys were cut and cleaned with acetone before the welding process.

Modified friction stir clinching (MFSC) and friction stir spot welding (FSSW) of the base alloys were carried out by changing material positioning to obtain AA2024-T3/AA5754-O and AA5754-O/AA2024-T3 joints. The MFSC is a two-step process that involves the creation of protuberance and keyhole at the 1st stage of the MFSC process (via the use of pin tool) and the elimination of protuberance and keyhole at the 2nd stage of the MFSC process (via the use of a pin-less tool). The appendix (see Fig. 30) shows the schematic illustration of the MFSC process. The morphologies and dimensions of the welding (HSS) tools employed for the FSSW and MFSC processes are shown in Fig. 1. Based on the preliminary experiments, the tool rotational speed was varied between 710 and 1400 rpm for the two processes (MFSC and FSSW) while the dwell time (5 s) and plunge depth (0.4 mm) were kept constant. The induced peak temperatures of the respective welding processes were measured via the use of a K-type thermocouple according to the illustration shown in Fig. 2.

The cross-sections of the MFSC and FSSW welded joints were obtained and subjected to standard metallographic procedures. The microstructural samples were etched in Barker's agent for 120 s at 20 V. The resultant structures of the joints were viewed under an optical microscope (OM), and scanning electron microscope (SEM). The average grain sizes of the MFSC and FSSW joints were obtained via Clemex image analysis. The microstructure was further characterized via the use of a transmission electron microscope (TEM). The tensile-shear and cross-tension loads of the MFSC and FSSW joints were obtained according

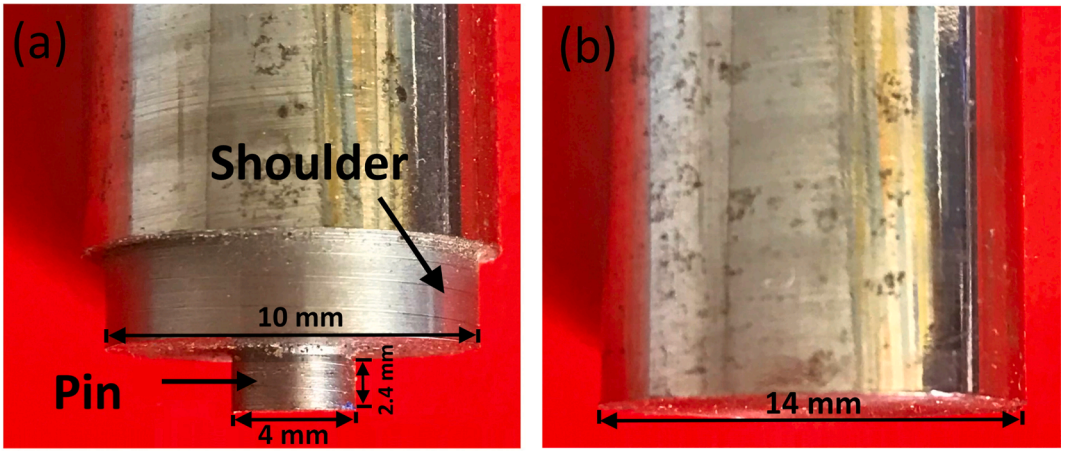

Fig. 1. Tools used for the welding process (a) FSSW and 1st stage of MFSC process, (b) second stage of MFSC process [26].

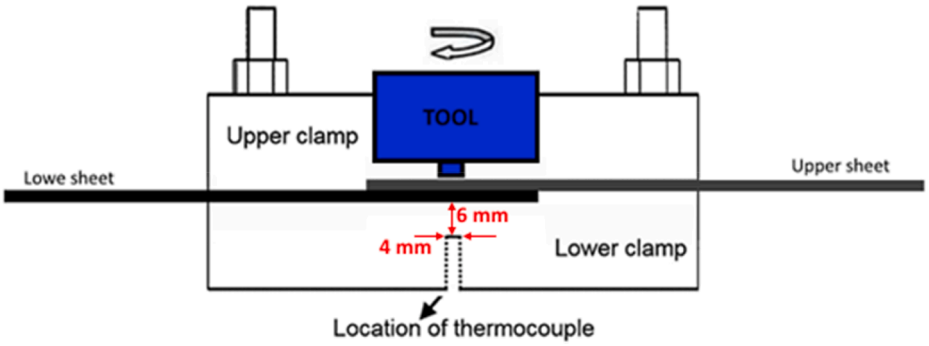

Fig. 2. Location of K-thermocouple during the FSSW and MFSC processes [27].

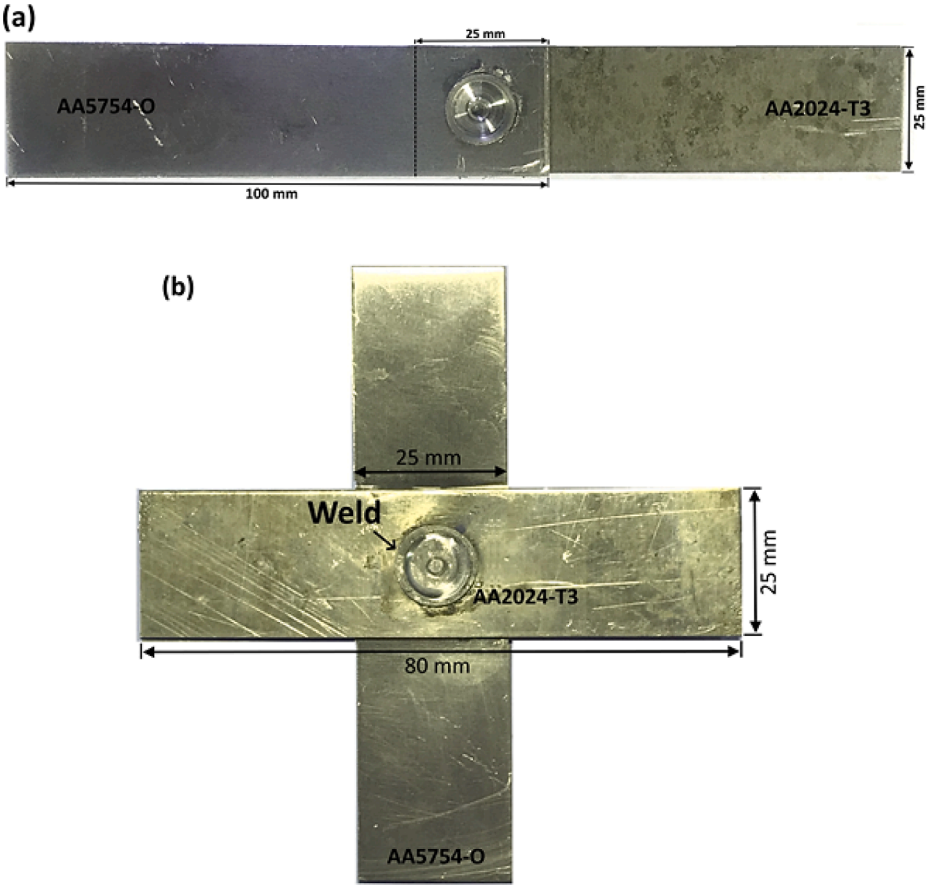

Fig. 3. The dimension of samples, (a) Tensile-shear test, (b) Cross-tension test.

to JIS Z3136 and JIS Z3137 standards respectively. Fig. 3 shows the dimensions of the tensile-shear and cross-tension samples employed for this study. The tensile test was carried out at a constant crosshead speed of 1 mm/min.

Results and discussion

Surface appearance and peak temperature

Tool profile-induced keyhole and protrusion are formed during the 1st stage of the MFSC process (see Appendix - Fig. 29) and the 2nd stage of the MFSC process eliminates these issues and also improves the bonded width. The top and bottom views of the MFSC welded AA2024-T3/AA5754-O and AA5754-O/AA2024-T3 joints (after the 2nd stage of the MFSC process) are shown in Figs. 4 and 5 respectively. The top views of the respective MFSC welds (see Fig. 4) reveal two kinds of geometric-differential flow-induced defects at the weld centers (due to the keyhole refilling effect) and the circumferential edges of the weld nuggets (due to the shoulder-induced cavity refilling effect). The level/width of the shoulder-induced cavity (at the nugget peripheral region) decreases as

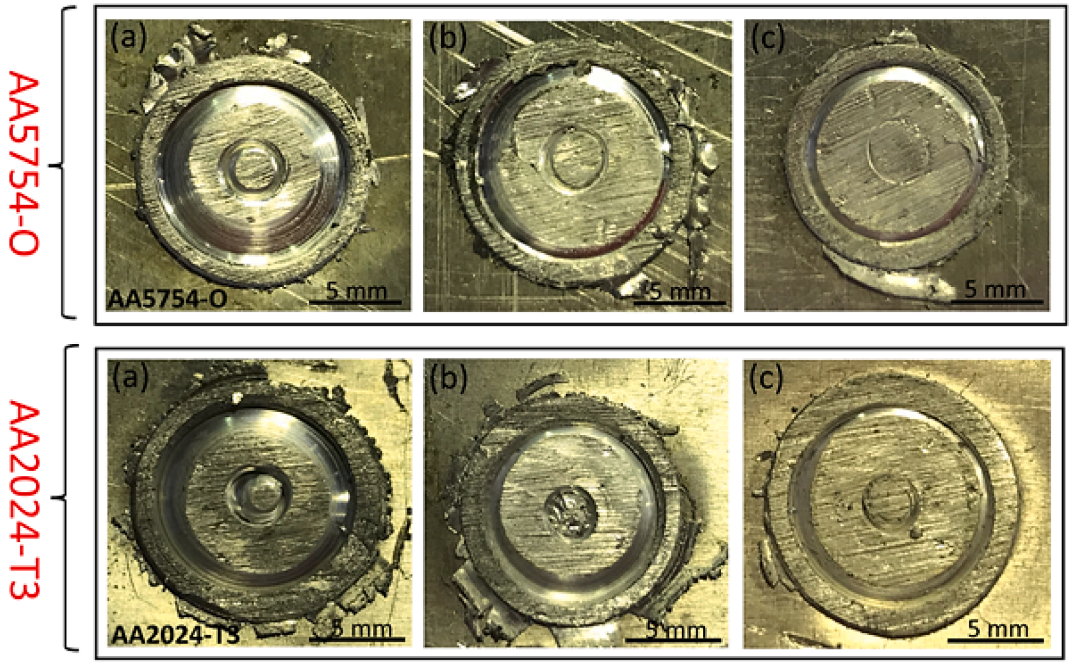

Fig. 4. Top views of 5754/2024 and 2024/5754 joints, (a) 710 rpm, (b) 1000 rpm, and (c) 1400 rpm.

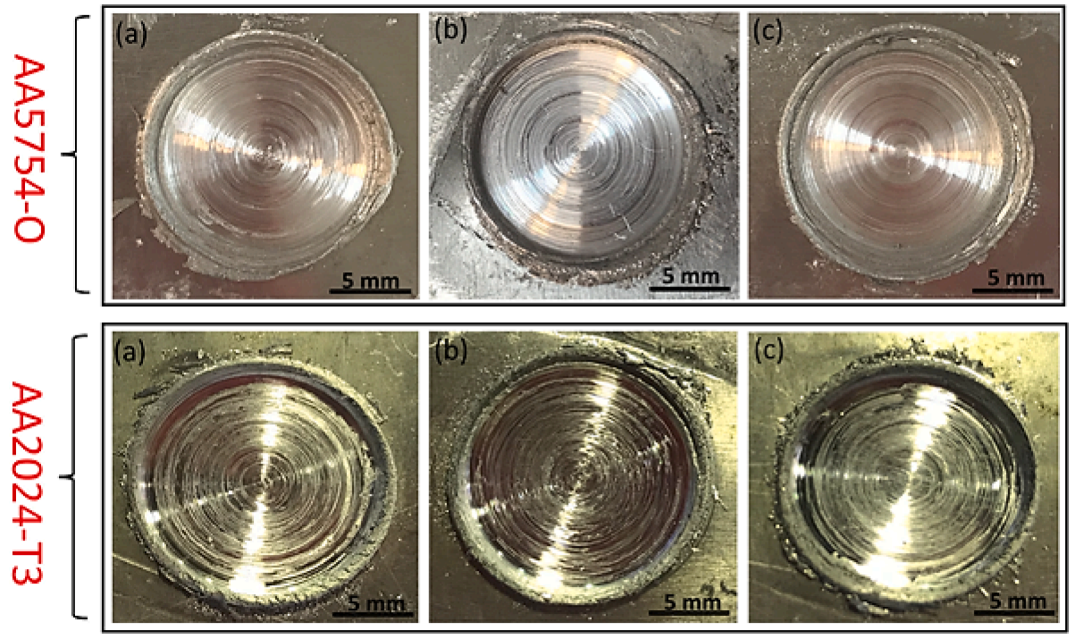

Fig. 5. Bottom views of 2024/5754 and 5754/2024 joints, (a) 710 rpm, (b) 1000 rpm, and (c) 1400 rpm.

the tool rotational speed is increased from 710 rpm to 1400 rpm (see Fig. 4). This occurrence is attributed to the improved local heat build-up (within the stir zone), better viscosity, and material flow as the tool rotational speed levels are increased. It is validated that a direct relationship exists between the peak temperature and tool rotational speed (see Fig. 6). Thus, a rise in the stir zone temperature is adjudged to have enhanced material flow to cutback the level/width of the shoulder-induced cavity in the MFSC welded joints. This finding also corroborates the works of Ebrahimzadeh et al. [28] as a combined upward-thrust flow, improved flowability, and intermingling are aided by an increase in the level of tool rotational speed. Fig. 5. reveals the bottom views of the MFSC welded AA2024-T3/AA5754-O and AA5754-O/AA2024-T3 joints. Pinless tool-induced circumferential (expelled) flash around the periphery of the weld nugget is palpable in all MFSC joints. An obvious disparity in the coloration of the bottom views is due to the different base materials. The cross-sections of the welds are

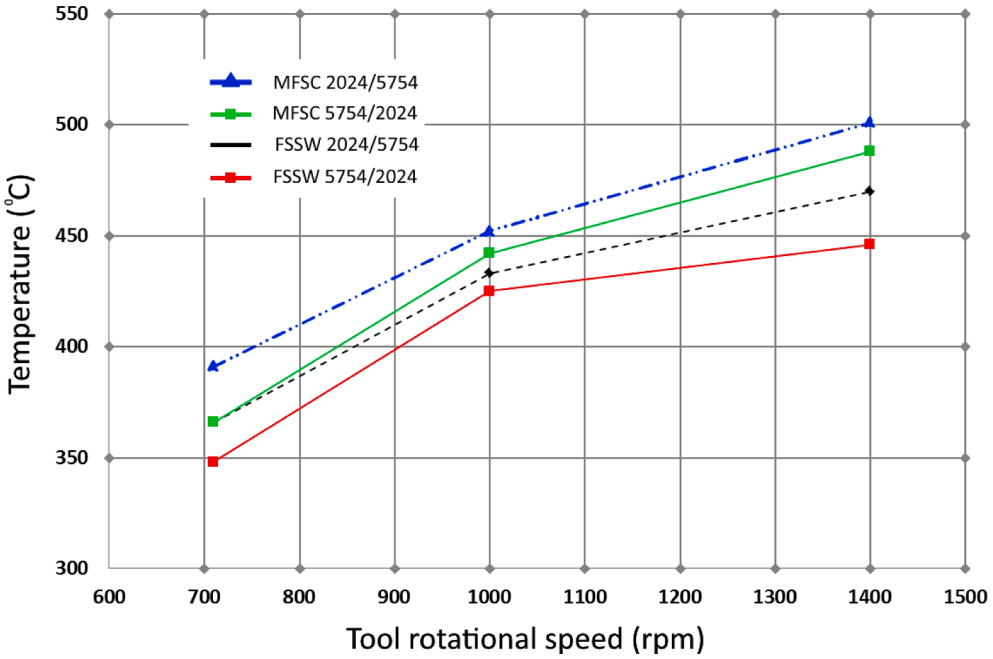

Fig. 6. Relationship between tool rotational speed and temperature as a function of material positioning.

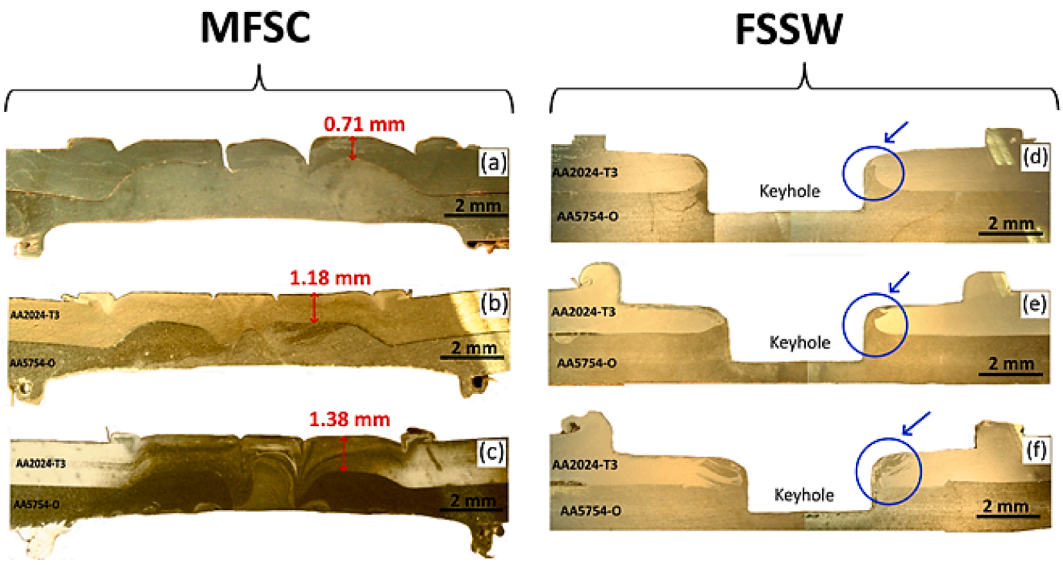

Fig. 7. Macrostructure of 2024/5754 joints, (a) 710 rpm, (b) 1000 rpm, and (c) 1400 rpm.

examined in section 3.2 to further clarify the MFSC welds (with different material positioning).

Fig. 6 reveals that material positioning influences the peak temperature of both the MFSC and FSSW welded joints. Maximum peak temperatures were obtained in the AA2024-T3/AA5754-O joints when compared to the AA5754-O/AA2024-T3 joints due to the material positioning effect. At a tool rotational speed of 1400 rpm, about 500 and 485 °C temperatures were obtained in the MFSC welded AA2024-T3/AA5754-O and AA5754-O/AA2024-T3 joints respectively while those of the FSSW joints were 475 and 442 °C respectively. This occurrence confirms that material positioning is a significant factor that affects the frictionally induced heat input in friction stir based welded joints. The plasticization strength (yield strength) of AA2024-T3 Al alloy is higher than that of AA5754-O Al alloy by a factor of about 1.62. This attribute indicates that material flow will commence at an earlier time in the AA5754-O Al alloy during the MFSC/FSSW process as compared to the AA2024-T3 Al alloy. The disparity in the properties of the base alloys is consequently viewed to be responsible for the difference in the attained peak temperatures between the AA2024-T3/AA5754-O and AA5754-O/AA2024-T3 joints. However, the reason for the higher peak temperature

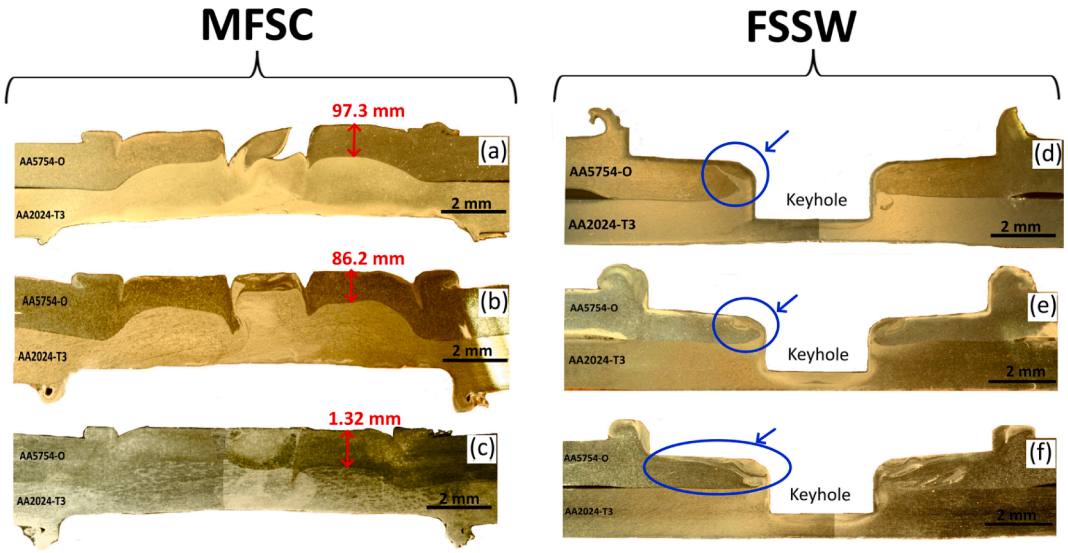

Fig. 8. Macrostructure of 5754/2024 joints, (a) 710 rpm, (b) 1000 rpm, and (c) 1400 rpm.

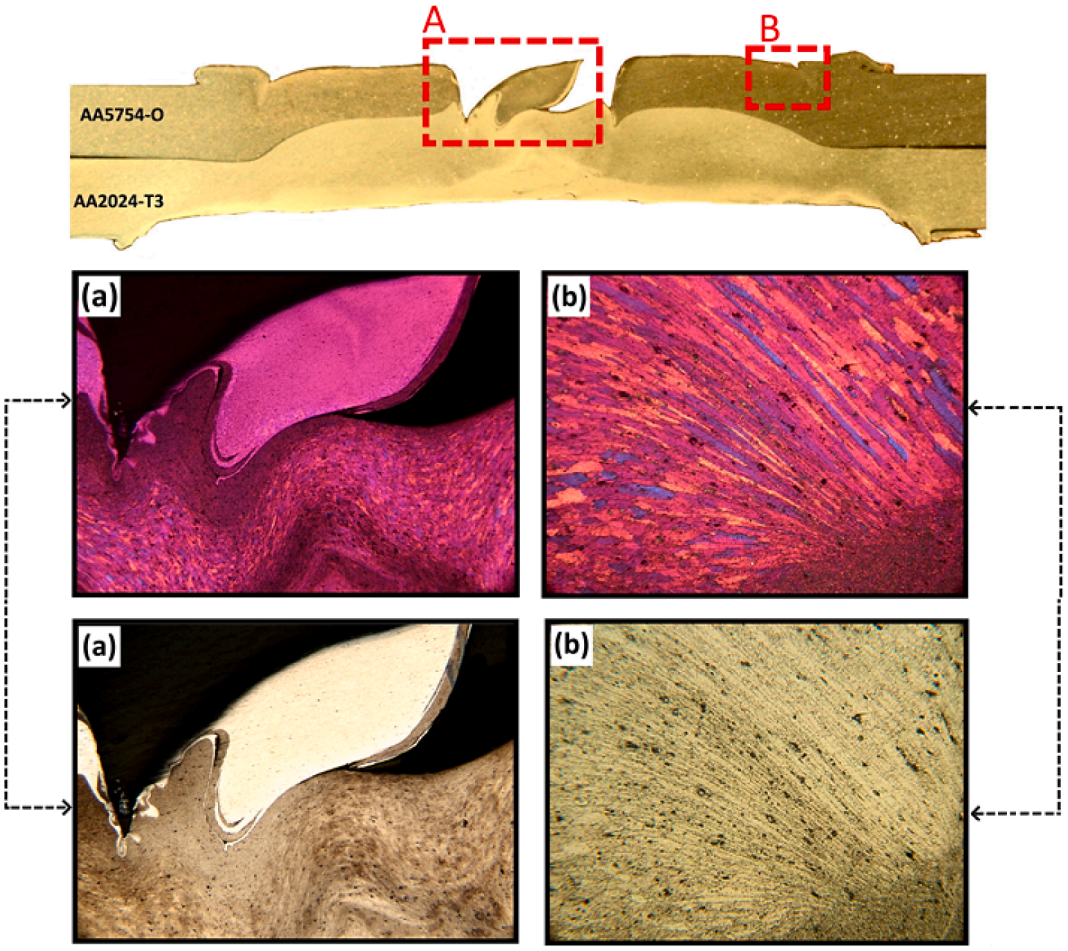

Fig. 9. Optical micrographs of the marked points "A" and "B" on the MFSC 5754/2024 joint obtained at 710 rpm (a) magnified view of point "A", (b) magnified view of point "B".

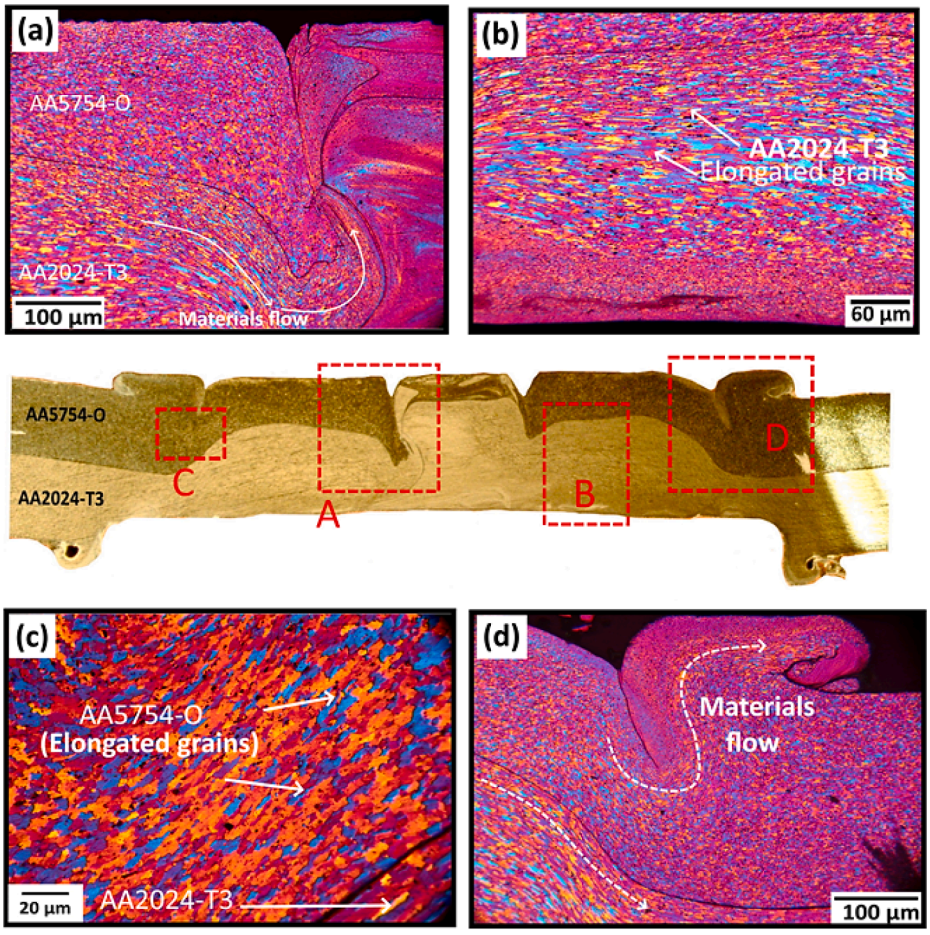

Fig. 10. Optical micrographs of the marked points on the macrograph of the MFSC 5754/2024 joint obtained at 1000 rpm, (a) magnified point "A", (b) point "B", (c) point "C", and (d) point "D".

in the MFSC joint as compared to the FSSW joint is attributed to the larger shoulder diameter employed for the 2nd stage of the MFSC process. The tool shoulder offers the dominant heat input during the friction stir welding process (generating about 75% of the heat input) [29]. As a result, a pinless tool is expected to induce a higher heat input and consequently a higher peak temperature than a pin tool. This phenomenon justifies the reason for a high temperature in the MFSC joint as compared to the FSSW joint.

Macrostructure

Figs. 7 and 8 show the cross-sections of the MFSC and the FSSW welded AA2024-T3/AA5754-O and AA5754-O/AA2024-T3 joints respectively. Obvious stress raisers (keyholes) are present in the FSSW joints while the presence of geometric-differential flow-induced defects (at the weld centers) is confirmed in the MFSC joints. An increase in the level of tool rotational speed reduces the level of this defect (in the MFSC joint) due to the improved material flow (associated with an increase in peak temperature) as revealed in Figs. 7a–c and 8a–c. The material positioning effect shows that the severity of the flow-induced weld center defect in the MFSC joints is intense in the AA5754-O/AA2024-T3 joints than the AA2024-T3/AA5754-O joints at low tool rotational speeds (710 and 1000 rpm). The weld center defect is improved as the tool rotational speed is increased irrespective of material positioning. Similarly, the disproportional plasticized thickness of the upper stirred sheet (in comparison to the stirred bottom part) ensues at the region closed to the refilled keyhole section at low tool rotational speed (710 rpm) in Figs. 7a and 8a. The thickness of the upper plasticized sheet rises in the AA2024-T3/AA5754-O joint (from 0.71 to 1.38 mm) as the tool rotational speed is increased (710–1400 rpm) while that of the AA5754-O/AA2024-T3 joints do not have a linear trend. On the other hand, the marked circular regions in Figs. 7d–f and 8d–f show the occurrence of upward material flow from the pin peripheral region towards the shoulder region in the FSSW joints. The level of inter-material mixing is somewhat higher in the marked (circular) regions as the tool rotational speed is increased to 1400 rpm (see Fig. 7f and 8f). This occurrence indicates that an increase in the level of tool rotational speed favors inter-material mixing in the FSSW joint.

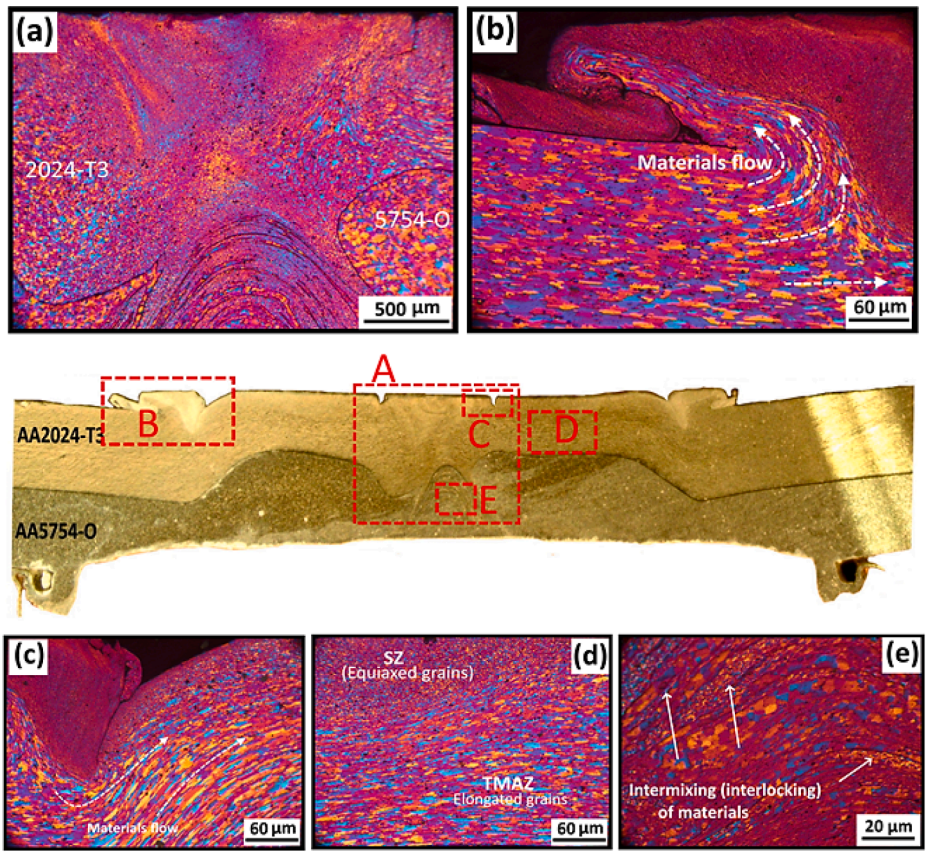

Fig. 11. Optical micrographs of the marked points on the macrograph of the MFSC 2024/5754 joint obtained at 1000 rpm, (a) magnified point "A", (b) point "B", (c) point "C", (d) point "D", and (e) point "E".

Material flow behavior

The close-up images of the MFSC and FSSW joints are examined to further clarify the inter-material flows of the joints as the welding parameters and material positioning are varied (see Figs. 9–16). Fig. 9 reveals that the plasticized AA2024-T3 alloy (bottom plate) does not significantly flow to refill the weld-center keyhole in the AA5754-O/AA2024-T3 joint (see region "A") at 710 rpm as compared to that of the AA2024-T3/AA5754-O joint. During the first stage of the MFSC process, thinning of the 5754-O Al alloy is adjudged to have ensued at the vortex region of the joint. The keyhole elimination process of the second stage of the MFSC process causes an upward thrust of the thinned 5754-O Al alloy (at the vortex zone) to leave an imperfectly filled keyhole at the weld center (at low tool rotational speed). This flow phenomenon is attributed to the reduced amount of frictionally induced heat input when harder and stronger material is utilized as the bottom plate. Meanwhile, region "B" of the joint shows stretched/elongated grains due to the thermomechanical effect of the welding process.

The upward material thrust (flow) is significantly improved at the weld center of the AA5754-O/AA2024-T3 joint as the tool rotational speed is increased to 1000 rpm in Fig. 10. The thinned AA5754-O Al alloy (at the vortex zone during the first stage of the MFSC process) flows upward with some plasticized AA2024-T3 Al alloy to refill the inherent tool-induced keyhole of the joint (an improvement over the observation in Fig. 9). This improvement is attributed to a better heat input (temperature) at 1000 rpm as compared to 710 rpm (as validated in Fig. 6). The Weld center keyhole is also sufficiently refilled in the AA2024-T3/AA5754-O joint (see Fig. 11). The comparison of the weld centers of the AA2024-T3/AA5754-O (see Fig. 11) and that of the AA5754-O/AA2024-T3 (see Fig. 10) obtained at 1000 rpm shows that material positioning dictates the material flow behavior in MFSC joint. Fig. 10a reveals an upward flow of the AA2024-T3 Al alloy with some flow-induced paths/lines indicating insufficient metallurgical bonding between the plasticized materials (upper and lower sheets) at the refilled keyhole section. On the other hand, Fig. 11a shows a good metallurgical bonding at the refilled keyhole section (see the marked region "A" in the macrograph). This implies that sufficient inter-material mixing and metallurgical bonding ensue when the harder material (AA2024-T3) is positioned as the upper plate during the MFSC process. However, the lower part of Fig. 11a shows a cluster of flow-induced paths. The magnification of this region (see the marked region "E") reveals the presence of an intercalated region which indicates the occurrence of intermixed and interlocked structures (see Fig. 11e). Other material flow behaviors in the nugget of the MFSC joints are indicated in Figs. 10 and 11. Elongated and equiaxed grains are present in the regions beneath the refilled shoulder-induced cavities (regions "C" and "D" in Fig. 10). Upward flow patterns (see region "B") are present at the refilled shoulder-induced cavities in Fig. 11b. On the other hand, Fig. 12 shows the MFSC joint obtained at a higher tool rotational speed (1400 rpm). The magnified regions of "A", "B", "C", "D", "E", and "F" are shown in

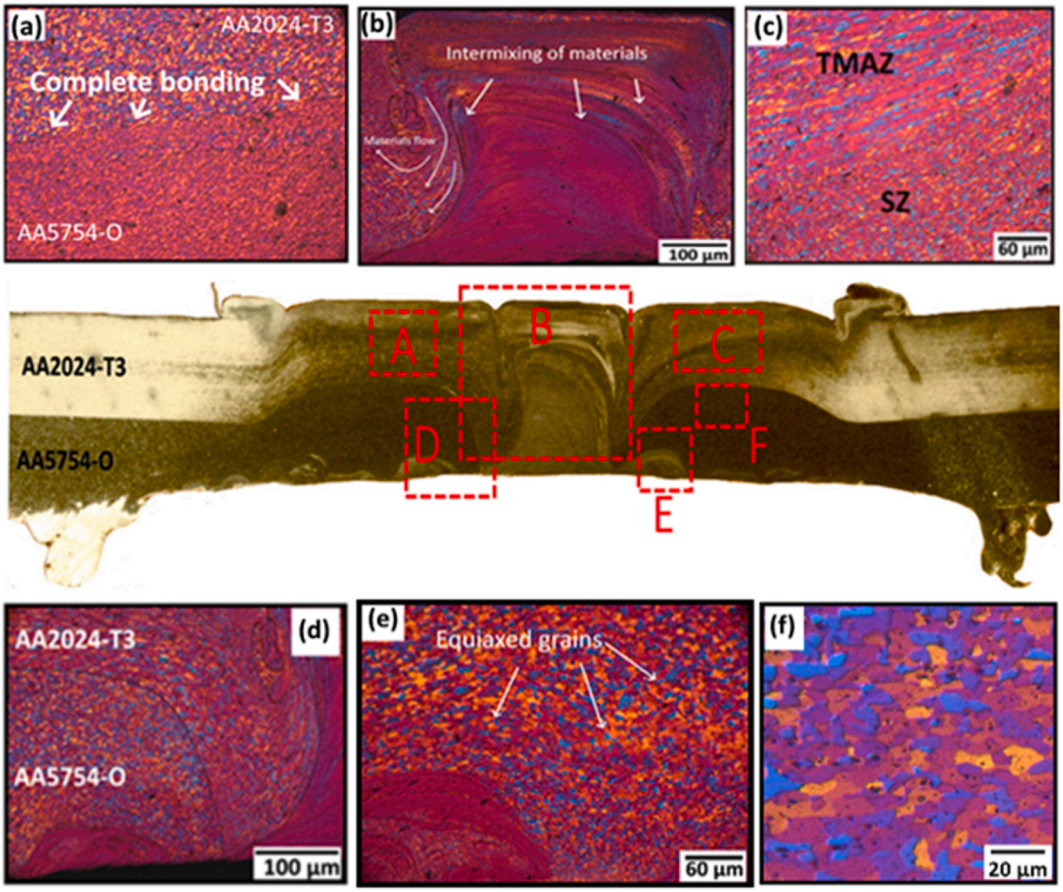

Fig. 12. Optical micrographs of the marked points on the macrograph of the MFSC 2024/5754 joint obtained at 1400 rpm, (a) magnified point "A", (b) point "B", (c) point "C", (d) point "D", and (e) point "E, and (f) point "F".

Fig. 12a–f respectively. The magnified refilled keyhole section (see region "B") is Fig. 12b. Evidence of complex flow with inter-mixing of materials is observed in this region (see Fig. 12b) while good metallurgical bonding (see region "A") is observed in Fig. 12a at a higher tool rotational speed.

In FSSW welds, the change in material positioning causes a change in the upward flow of the lower material into the upper material while the inherent hooking profile exists in all the FSSW welds (Figs. 13a, 14a, 15a, and 16a). At tool rotational speed of 710 rpm, the upward flow of material into the upper material (see regions "B" and "D" magnified as Fig. 13b and d respectively in Fig. 13) is not as intense as that of the joint obtained at higher tool rotational speeds (1000 and 1400 rpm) irrespective of the position of materials. The stir zones of the joint reveal equiaxed grain structures in all weld nuggets. Figs. 14 and 15 compare the FSSW joints with different material positioning obtained at 1000 rpm. Regions "B" (see Fig. 14b) and "D" (see Fig. 14d) in Fig. 14 reveal the flow of lower material (harder material) into the upper material (soft) to form intercalated bands at the shoulder-keyhole region in the MFSC 5754/2024 joint. This occurrence is due to the extruding material flow-induced action of the tool pin. However, such flow-induced structure is restrained when the upper plate is harder than the lower plate in MFSC 2024/5754 joint as evidence of similar regions "B" (see the magnified region in Fig. 15b) and "D" "B" (see the magnified region in Fig. 15d) show no similar flow pattern in Fig. 15. This also confirms that material positioning alters the material flow behavior in the FSSW joint. As the tool rotational speed is increased to 1400 rpm, similar flow-induced intercalated structure (with a larger surface area) is found at the shoulder-pin region (see regions "C" and "B" as Fig. 16c and b respectively) in the MFSC 5754/2024 joint. This occurrence implies that higher heat input (at a high tool rotational speed of 1400 rpm) reduces the viscosity of the material and facilitates inter-material flow at the shoulder-pin region. Equiaxed grains ensue in the joint due to dynamic recrystallization.

Microstructure

The appendix shows the rolling process-induced elongated grains of the base Al alloys (AA5754-O and AA2024-T3). The SZ, TMAZ, and HAZ of the welds are shown in Fig. 17. The images reveal evenly dispersed equiaxed grains at the SZ (see Fig. 17a–d), coarse grains at the TMAZ (see Fig. 17e–h), and coarser grains at the HAZ (see Fig. 17i–l). Severe plastic deformation at the weld nugget zone or SZ leads to the formation of fine and homogeneous equiaxed crystals (in Fig. 17a–d) due to the occurrence of dynamic recrystallization phenomenon at the SZ aided by the induced peak/maximum temperature and strain [25]. The grain refinement approaches/mechanisms in this case (joint) are termed as the continuous dynamic recrystallizations as a result of the high stacking fault energy of Al and the dislocation accumulation-aided nucleation of

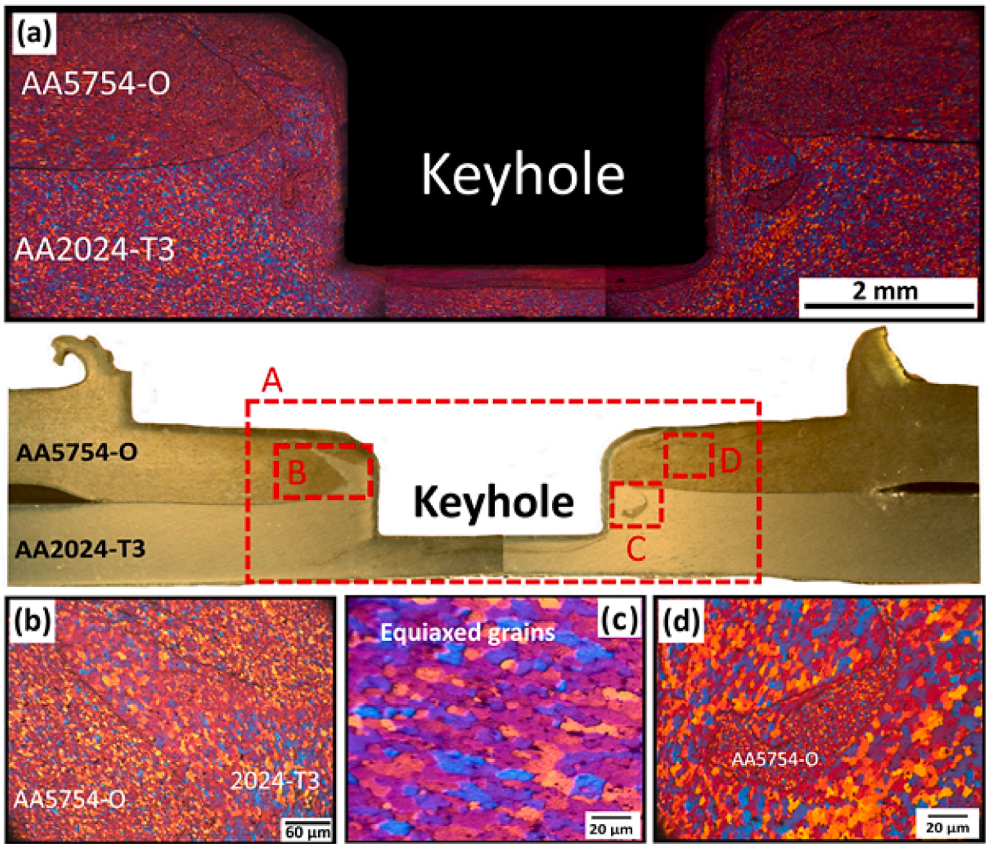

Fig. 13. Optical micrographs of FSSW 5754/2024 joint at 710 rpm, (a) magnified region "A", (b) region "B", (c) region "C", (d) region "D".

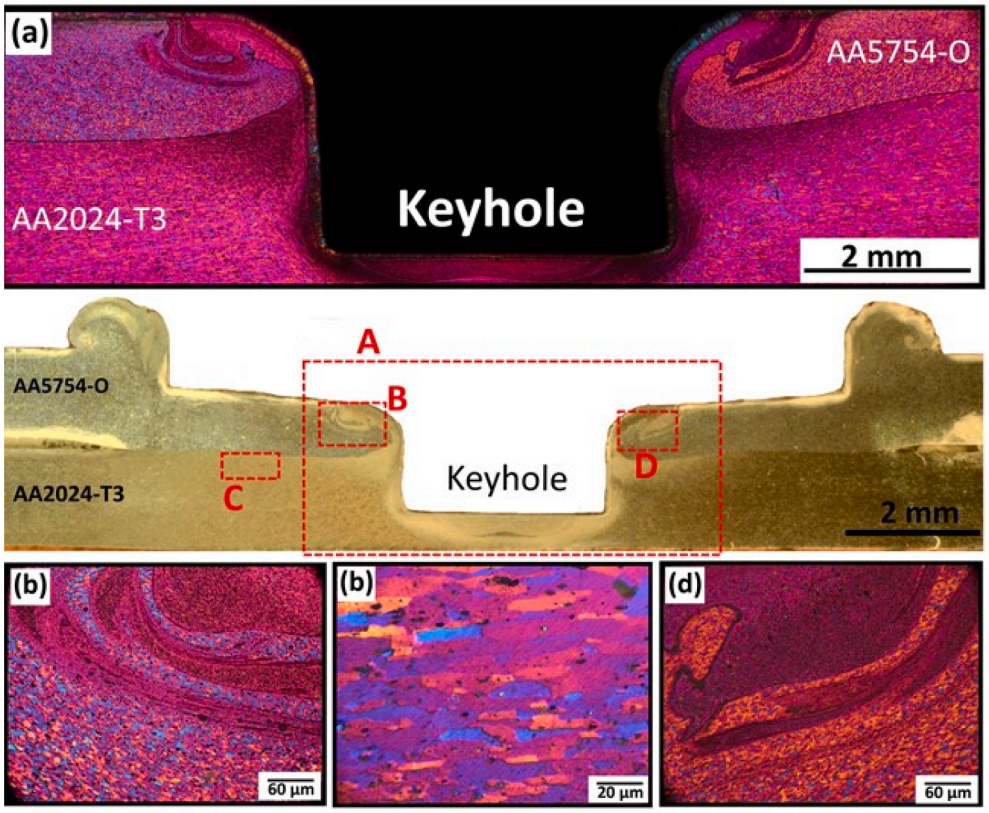

Fig. 14. Optical micrographs of FSSW 5754/2024 joint at 1000 rpm, (a) magnified region "A", (b) region "B", (c) region "C", (d) region "D".

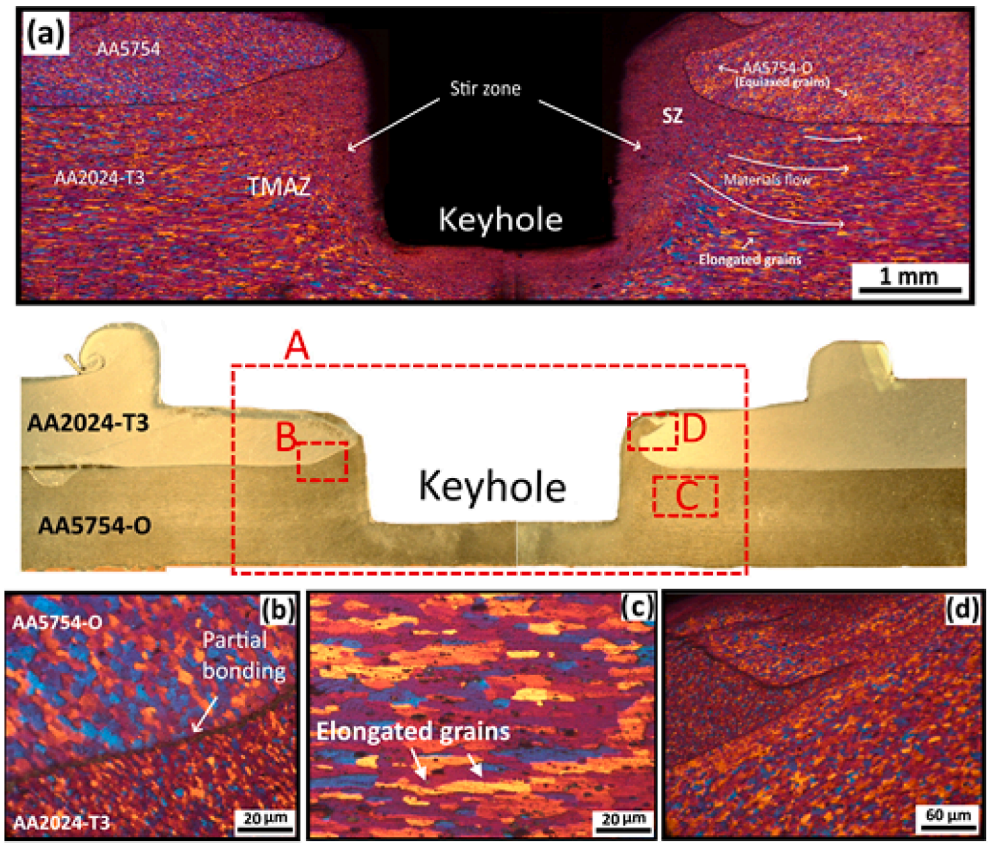

Fig. 15. Optical micrographs of FSSW 2024/5754 joint at 1000 rpm, (a) magnified region "A", (b) region "B", (c) region "C", (d) region "D".

recrystallization [30]. The induced dislocations at the sub-grains and low angle grain boundaries (LAGBs) aid the continuous transformation into high angle grain boundaries and consequently fine equiaxed grain structure at the SZ during the welding process [30]. Accumulated dislocation-induced nucleation of recrystallization may also cause the formation of ultrafine grains in the highly strained sections of the SZ.

The different and close-packed grains at the SZ indicate diverse grain orientations and the existence of a high level of grain boundary misorientation angle. Meanwhile, a direct relationship exists between grain boundary energy and grain boundary misorientation angle. This shows that more energy will be needed to induce and propagate micro-crack in the SZ (large-angle grain boundaries) [31]. Localized strain concentration can be said to exist at the grain boundaries of the TMAZ and HAZ while a relaxed strain is reported by Liu et al. [32] to ensue within grains owing to dislocation release (attributed to partial precipitated phase dissolution into the Al matrix). The low amount (density) of precipitated phases inside the grains inhibits strain localization within grains. The higher amount of strains at the grain boundaries of the TMAZ and HAZ are thus attributed to mechanical stirring-precipitation and thermal effects respectively. Strain localization has also been revealed to be dominant at the region along with the coarse phases (second), sub-grain and grain boundaries in the TMAZ of the friction stir welded 7050-T7451 Al joint [32]. This implies that shear textural components are the characteristic textures of the friction stir processed joints since a direct relationship exists between induced strain and shear textural component [33]. The average misorientation angle had been reported to increase from the base metal (BM) to the HAZ and the SZ while the proportion of the low angle grain boundary (LAGBs) showed a decrease from the BM to the HAZ and the SZ [34].

Fig. 18 indicates the SZ structures of the MFSC welded joints as the tool rotational speed is increased from 710 to 1400 rpm. The coarseness of grains is observed as the rotational speed is increased. The average grain sizes of the welds are measured to quantitatively correlate the grain sizes in the SZs with the tool rotational speeds (see Fig. 19). The average grain sizes of the AA5754-O and AA2024-T3 Al alloys (base metals) are 35 and 60 µm respectively while the average grain sizes of both the MFSC and FSSW joints under different tool rotational speeds and material positioning are provided in Fig. 19. An increase in the tool rotational speed (710–1400 rpm) causes a rise in the average grain sizes of all joints (see Fig. 19a and b) irrespective of the type of joint or the position of materials. Grain increments of 4.12–6.88 µm and 3.99–6.37 µm were obtained in the MFSC welded AA2024-T3/AA5754-O and AA5754-O/AA2024-T3 joints respectively while increments of 3.29–5.73 µm and 3.11–5.13 µm were obtained in the FSSW welded AA2024-T3/AA5754-O and AA5754-O/AA2024-T3 joints (as the tool rotational speed is increased from 710 to 1400 rpm). The direct correlation between heat input and tool rotational speed is responsible for the increase in the average grain sizes of the welds. A rise in heat input favors grain coarsening and this evidence is revealed in Fig. 19 as the tool rotational speed (heat input/peak temperature) is increased.

Material positioning also greatly influences the average grain sizes of the welds. Larger grain sizes are observed in the AA2024-T3/AA5754-O

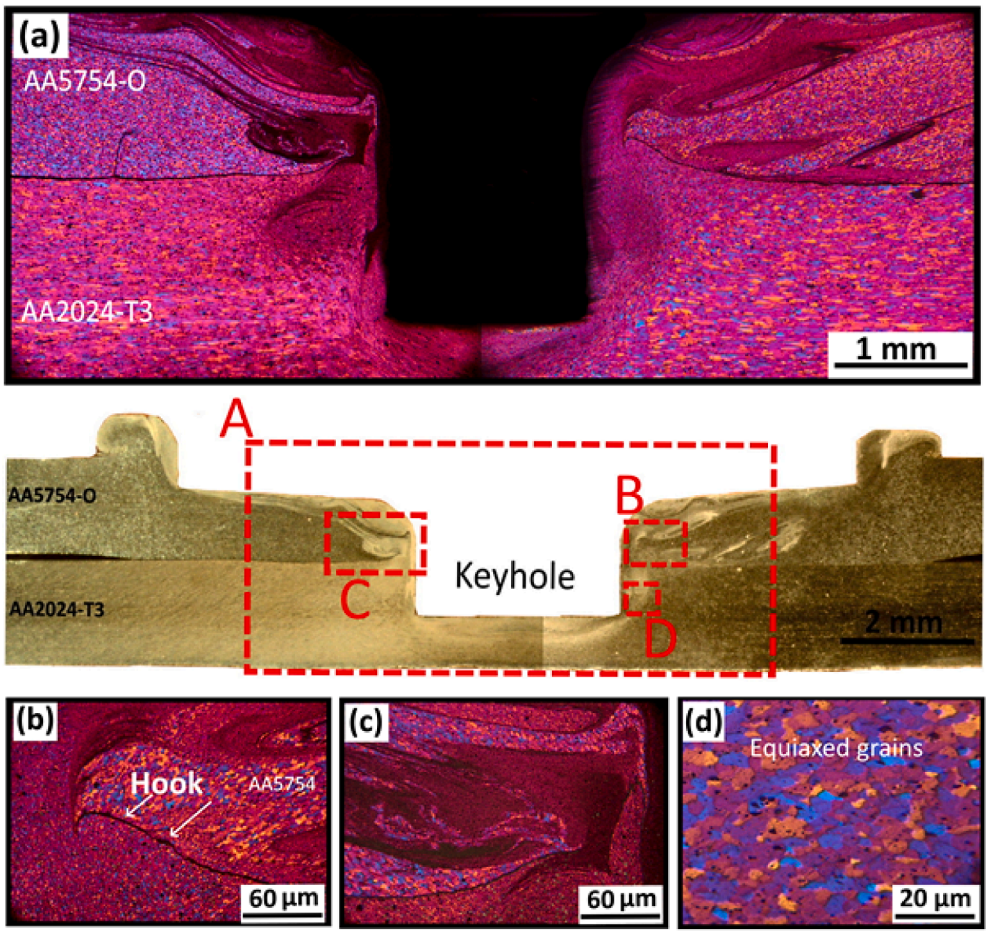

Fig. 16. Optical micrographs of FSSW 5754/2024 joint at 1400 rpm, (a) magnified region "A", (b) region "B", (c) region "C", (d) region "D".

joints (MFSC and FSSW) when compared to the AA5754-O/AA2024-T3 joints in Fig. 19. Grain sizes of 4.12 μm and 3.99 μm were obtained at the SZs of the MFSC welded AA2024-T3/AA5754-O and AA5754-O/AA2024-T3 joints respectively (at 710 rpm) while 3.29 μm and 3.11 μm were obtained in the FSSW welded counterparts. The disparity in the material properties is adjudged to have influenced the changes in the average grain sizes of the joints as the material positioning is changed. The reason for the presence of larger grain sizes in the MFSC welded joints (as compared to the FSSW welded joint) is due to the two-fold recrystallization attribute of the MFSC process and the use of a larger shoulder (pinless) tool (dominant heat input is generated at the tool shoulder). The overall heat input from the MFSC process is thus greater than that of the FSSW process and this behavior is reckoned to be responsible for the larger grain sizes in the MFSC joints.

The TEM images of the welded (MFSC and FSSW) joints were examined to further understand the effect of material positioning on the weld structure. The stir zones (sampling locations) of the joints are presented in Fig. 20. It has been reported that the AA5754 substrate contains Al_3Mg_2 and Mg_2Si phases while the AA2024-T3 substrate has AlCu, Al_2Cu, $AlCu_4$, and Cu_9Al_4 phases [35]. These phases are inevitable in the interface between the dissimilar alloys. Evidence of precipitated phases is present in all categories of the joints. A disparity in the density of dislocation is observed in Fig. 20 due to the material positioning effect and different welding processes. The low density of dislocations (see Fig. 20a) and dislocation tangles (see Fig. 20b) are present in the MFSC welded AA5754-O/AA2024-T3 and AA2024-T3/AA5754-O joints respectively.

A network of dislocation lines (bending) is also present in Fig. 20b. On the other hand, the FSSW welded AA2024-T3/AA5754-O joint (see Fig. 20c) has a combination of low dislocation density, a small area fraction of dislocation tangles, and ultrafine precipitated phases whereas that of the AA5754-O/AA2024-T3 joint also reveals finely dispersed ultrafine precipitated phases, a few coarsened phases, and no palpable dislocation tangles (see Fig. 20d). Thus, it can be concluded that AA2024-T3/AA5754-O weld arrangement favors the formation of dislocation tangles when compared to AA5754-O/AA2024-T3.

Tensile failure load of joints

Fig. 21 provides the cross tension and tensile-shear loads of the MFSC and FSSW joints obtained with different material positioning and at different tool rotational speeds (710–1400 rpm). Due to the tool rotational increase, the cross-tension loads of the AA5754-O/AA2024-T3 joints are increased from 3089 to 3697 N, and from 2566 to 3369 N after MFSC and FSSW processes respectively (see Fig. 21a) whereas those of AA2024-T3/AA5754-O joints also increased from 3207 to 3617

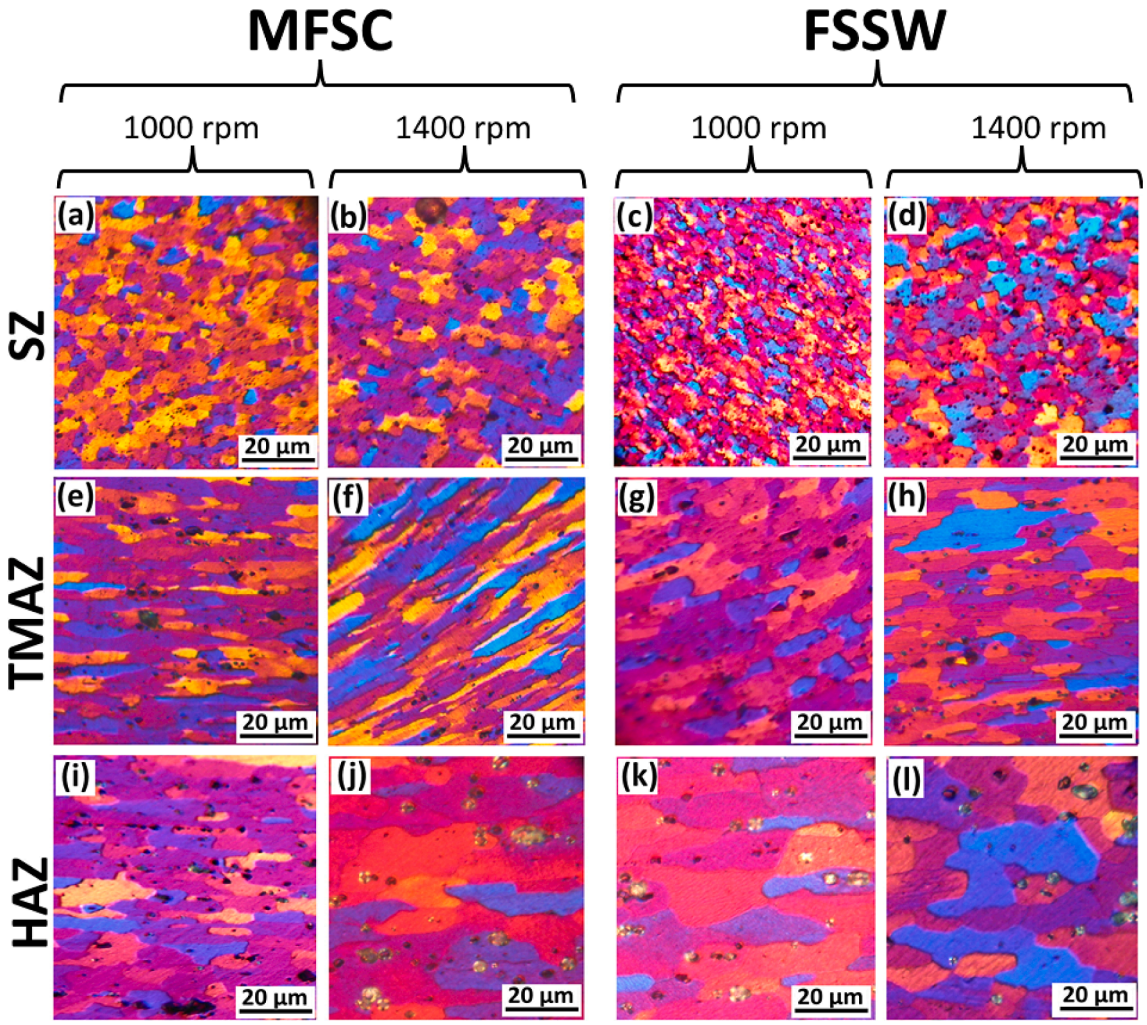

Fig. 17. Weld zones of the MFSC and FSSW 2024/5754 joints produced at 1000 and 1400 rpm, (a)-(d) Stir zones (SZs), (e)-(h) Thermomechanical affected zones (TMAZs), (i)-(l) Heat affected zones (HAZs)).

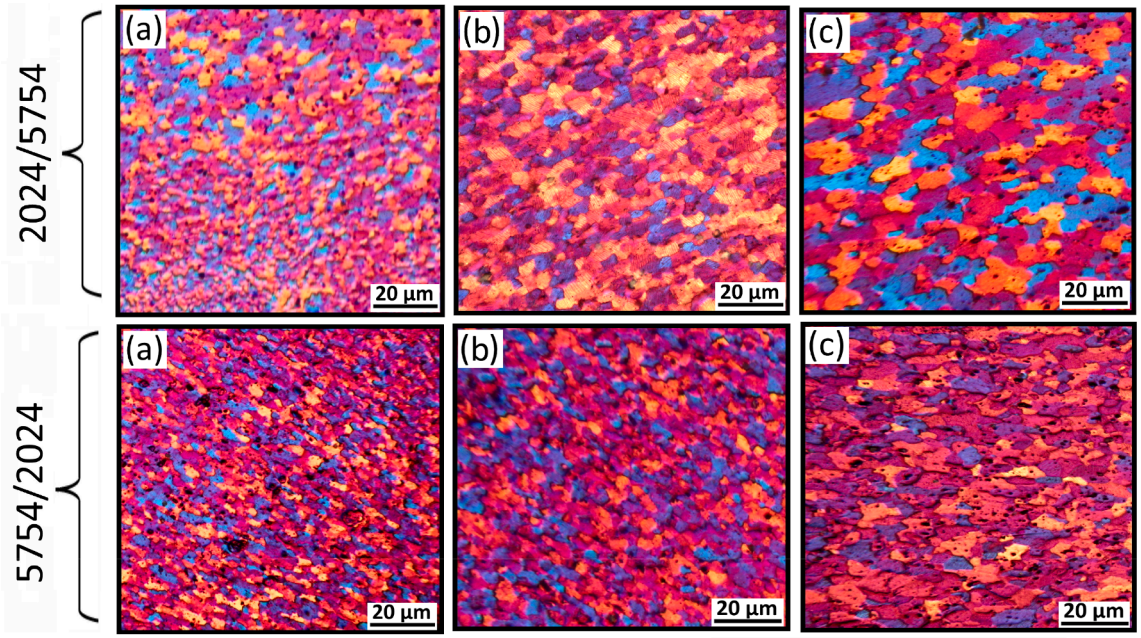

Fig. 18. SZ structure of the MFSC joint as a function of tool rotational speed and materials positioning, (a) 710 rpm, (b) 1000 rpm, and (c) 1400 rpm.

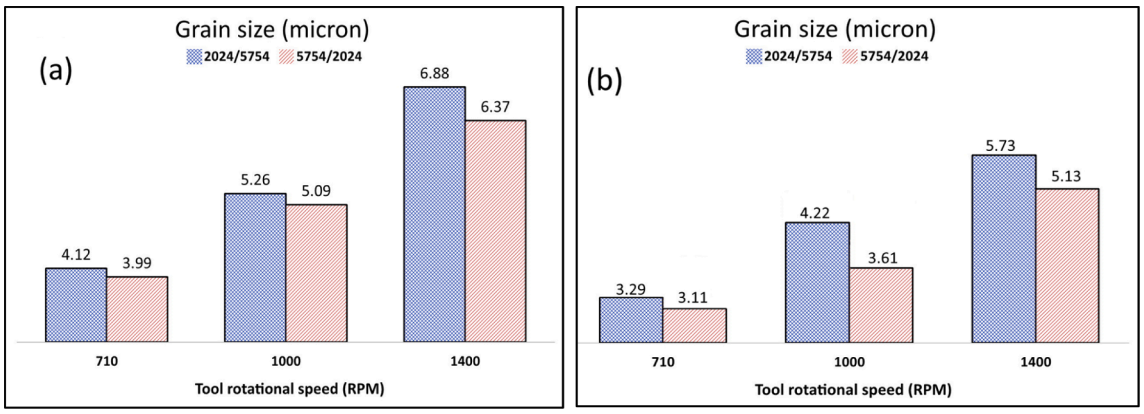

Fig. 19. Average grain sizes in the joints (a) MFSC and (b) FSSW.

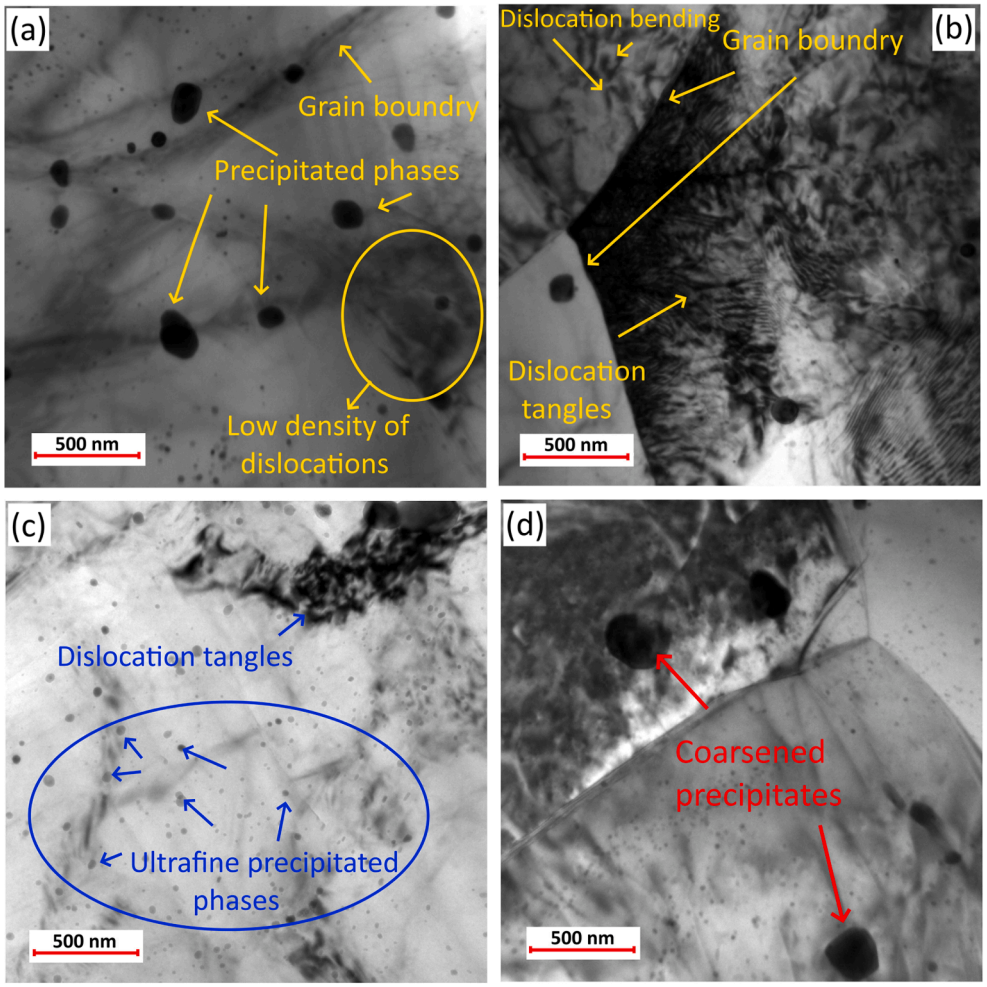

Fig. 20. TEM images of the stir zones of (a) MFSC welded AA5754-O/AA2024-T3 (1000 rpm), (b) MFSC welded AA2024-T3/AA5754-O (1000 rpm), (c) FSSW welded AA2024-T3/AA5754-O (1000 rpm), (d) FSSW welded AA5754-O/AA2024-T3 (1000 rpm) joints.

N and 2612-3286 respectively (see Fig. 21c). The tensile-shear loads of the AA2024-T3/AA5754-O joints increased from 5010 to 6317 N (MFSC joints) and 4236–5398 N (FSSW joints) as shown in Fig. 21d while those of the AA5754-O/AA2024-T3 joints increased from 4862 to 5366 N (MFSC joints) and 3936–4718 N (FSSW joints) respectively in Fig. 21c. Thus, it can be concluded that an upsurge in the tool rotational speed increases the tensile loads of all the joint categories due to the increase in heat/thermal input leading to better inter-material mixing and metallurgical bonding between the plates. This observation has also been attributed to an improvement in the stir zone width and bonded length in the studies of Zhang et al. [27]. Similarly, the reduction in the severity of flow-induced defects as the tool rotational speed was increased was

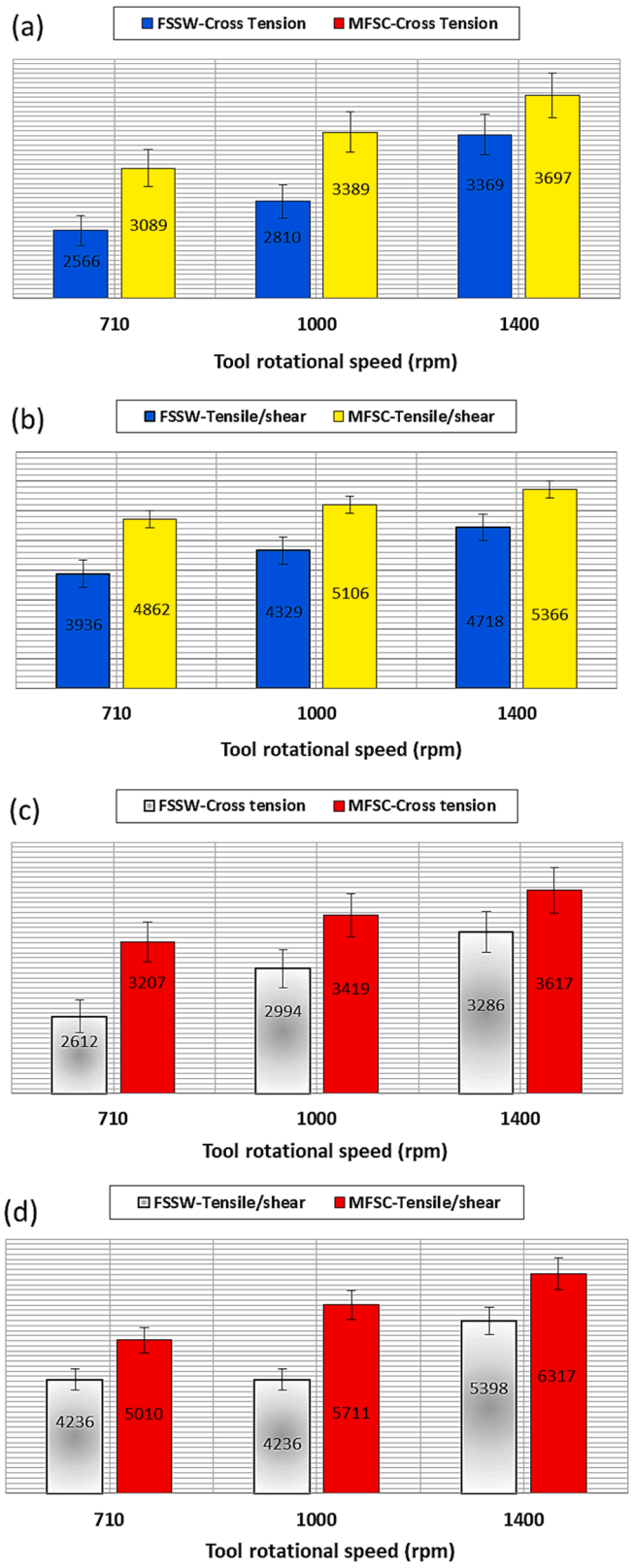

Fig. 21. Cross-tension and Tensile-shear failure loads of the welded joints (a) and (b) 5754/2024, (c), and (d) 2024/5754.

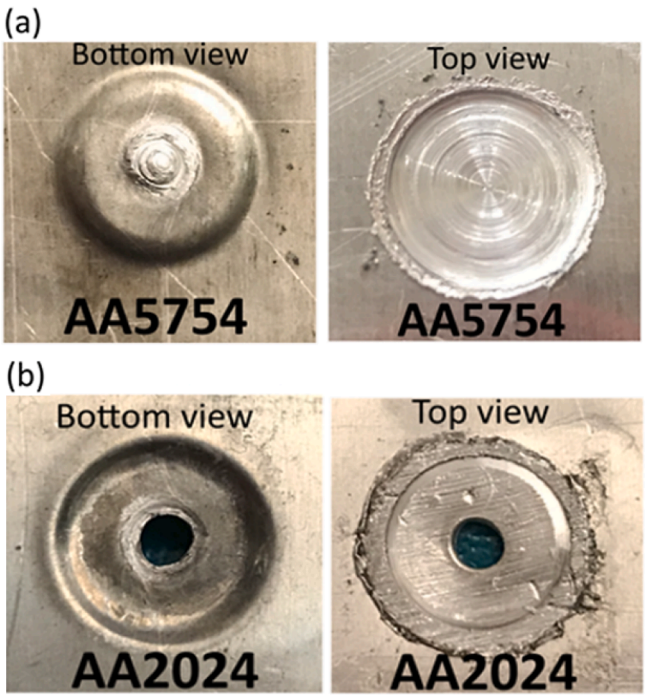

Fig. 22. Fractured MFSC welded 2024/5754 joint at low rotational speed (710 rpm).

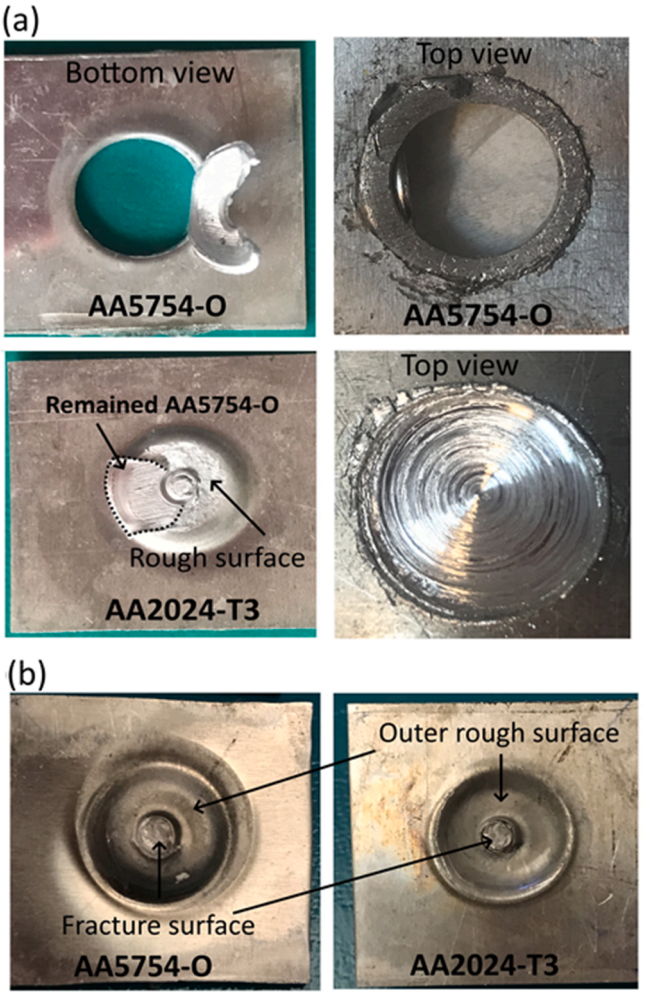

Fig. 23. Fracture modes as a function of materials positioning, (a) AA5754-O/AA2024-T3, (b) AA2024-T3/AA5754-O.

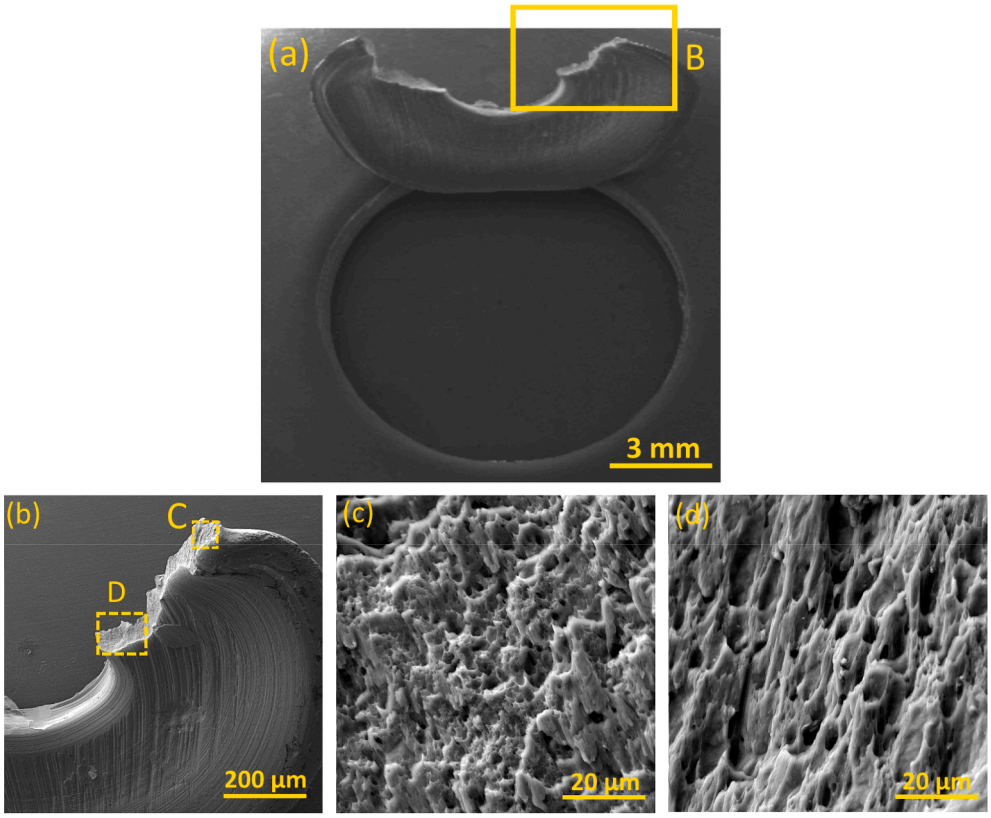

Fig. 24. Fracture SEM-SE images of AA5754/AA2024 weld (AA5754 side).

linked to the direct relationship between the weld failure resistance and tool rotational speed in the works of Paidar et al. [21]. A rise in the average grain sizes (as the tool rotational speed is increased in Fig. 19) does not play a dominant influence on the tensile load of the joints.

The AA2024-T3/AA5754-O joint produced higher failure resistances (cross-tension and tensile shear) when compared to the AA5754-O/AA2024-T3 joint in both joining methods (FSSW and MFSC). Maximum tensile shear loads of 6317 N and 5366 N were obtained in the MFSC AA2024-T3/AA5754-O and AA5754-O/AA2024-T3 joints respectively while the FSSW joints had 5398 N and 4718 N, respectively. This occurrence is due to the disparities between the material flow stresses and the in-nugget dislocation densities during the welding process. The presence of relatively high dislocation density and tangles in the AA2024-T3/AA5754-O joint is a salient factor responsible for the improved strength of the joint. These features are adjudged to have hindered slip during the tensile loading process and as such improved the failure resistance of the AA2024-T3/AA5754-O joints when compared with the AA5754-O/AA2024-T3 joints. Li et al. [31] also revealed that deformation slips are further impeded by the presence of fine secondary precipitates and LAGBs. Tan et al. [36] corroborated that a decrease in the density of dislocation decreased the tensile strength of the as-welded AA3003 Al alloy while a combination of grain refinement and high dislocation density improved the performance of the joint. However, the presence of a larger bonded width/area in the MFSC joints is responsible for the improved fracture resistance in the MFSC joint as compared to the FSSW joint. The effective bond area of the FSSW joints is reduced by the presence of an inherent keyhole within the weld nugget. This feature acts as a stress raiser during the tensile loading process and it eventually lowers the fracture resistance of the joint.

Fractography

It should be pointed out that similar fracture profiles of the MFSC joints were obtained irrespective of the material positioning at low tool rotational speed (710 rpm). As a result, Fig. 22 alone was used to explain the fracture of the MFSC joint (at low rotational speed). The presence of partially refilled keyholes (owing to geometric-differential flow) at the centers of both the MFSC AA2024-T3/AA5754-O and AA5754-O/AA2024-T3 joints (at 710 rpm) acts as a stress concentration site during the axial loading processes of the joints.

This attribute aids the removal of the refilled (and plasticized) mass from the inherent keyhole (to leave a hole at the top AA2024 plate) and it is thus responsible for the observed fracture profile in Fig. 22. The bottom view of the AA5754 side (see Fig. 22a) reveals that the circumferential surrounding/area close to the partially refilled region is smooth. This observation indicates that efficient intermixing/intermingling of materials is hindered at low rotational speed due to the low amount of frictionally generated heat input.

Material positioning alters the fracture pattern in the MFSC welds as the tool rotational speed is increased. Fig. 23 reveals the fracture

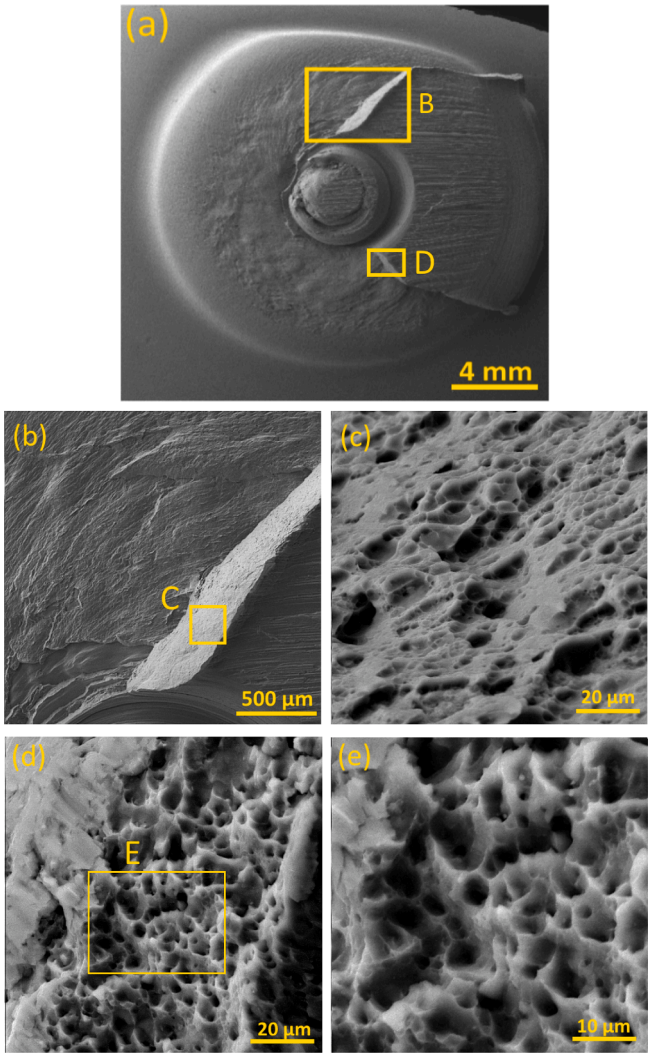

Fig. 25. Fracture SEM-SE images of AA5754-O/AA2024-T3 weld (AA2024 side).

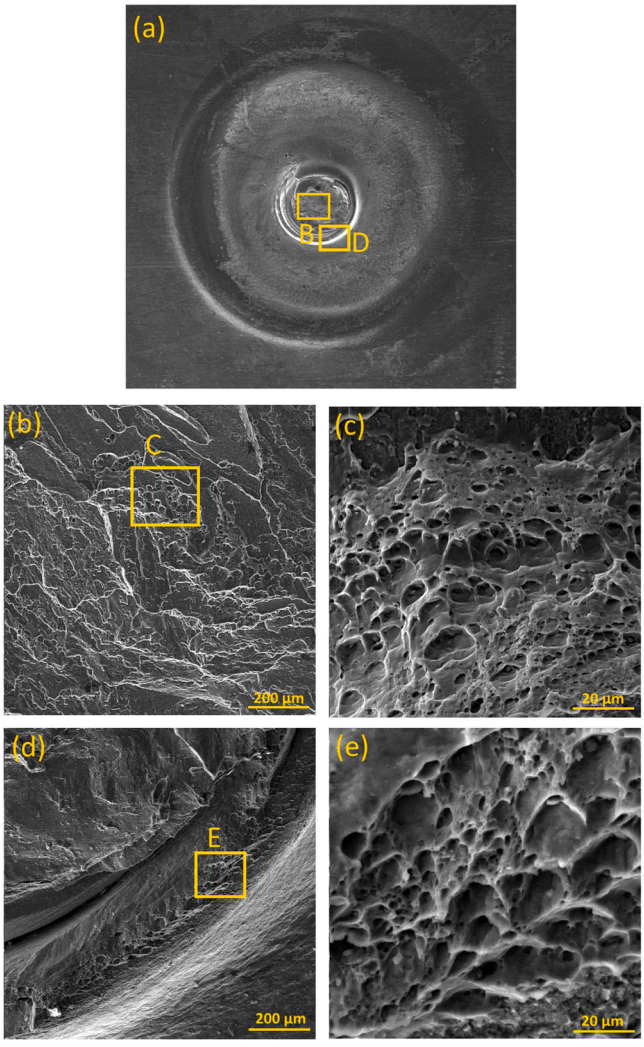

Fig. 26. Fracture SEM-SE images of AA2024-T3/AA5754-O weld (2024 side).

samples of the joints as the tool rotational speed is further increased. Two different fracture modes are obtained in the MFSC joints in Fig. 23. The first category is the nugget-tear off and the second is the refilled center-aided fracture morphologies. To understand the fracture mode, the close-up images of the fracture surfaces are further examined in SEM (see Figs. 24–27). The magnified fracture regions of the AA5754 and AA2024 sides in the MFSC AA5754-O/AA2024-T3 joints are shown in Figs. 24 and 25 respectively. The presence of dimple structures along the fracture paths (see marked and magnified regions "C" and "D" in Fig. 24 and regions "B" and "D" in Fig. 25a) depicts the occurrence of ductile fracture behavior at the plasticized and recrystallized zone of the joint [37,38] (Fig. 28.).

Figs. 26 and 27 reveal the fracture surfaces of the second fracture mode at the 2024 and 5754 sides respectively. This fractography shows that the axial tensile load is perpendicular to fracture surfaces. Shallow dimples are present in Fig. 26b and c and these indicate that the plastic deformation regions "B" (see Fig. 26a) and "C" (see Fig. 27a) are limited. At higher magnifications, shallow dimples are palpable in Fig. 26c and d respectively. Such observation has been attributed to the dynamic recrystallization effect and the presence of an equiaxed second phases in the studies of Guo et al. [39].

Conclusion

The effects of tool rotational speed and material positioning (material flow influencing parameters) on modified friction stir clinching of AA2024-T3 and AA5754-O Al alloys have been successfully investigated. The findings of this paper are summarized as follow:

i. Low tool rotational speed promotes the formation of partial weld-center (refilling) defects in the MFSC joints due to the geometric-differential flow effect.
ii. Weld-centre defect is severe in the AA5754-O/AA2024-T3 as compared to the AA2024-T3/AA5754-O joints at low tool rotational speed.

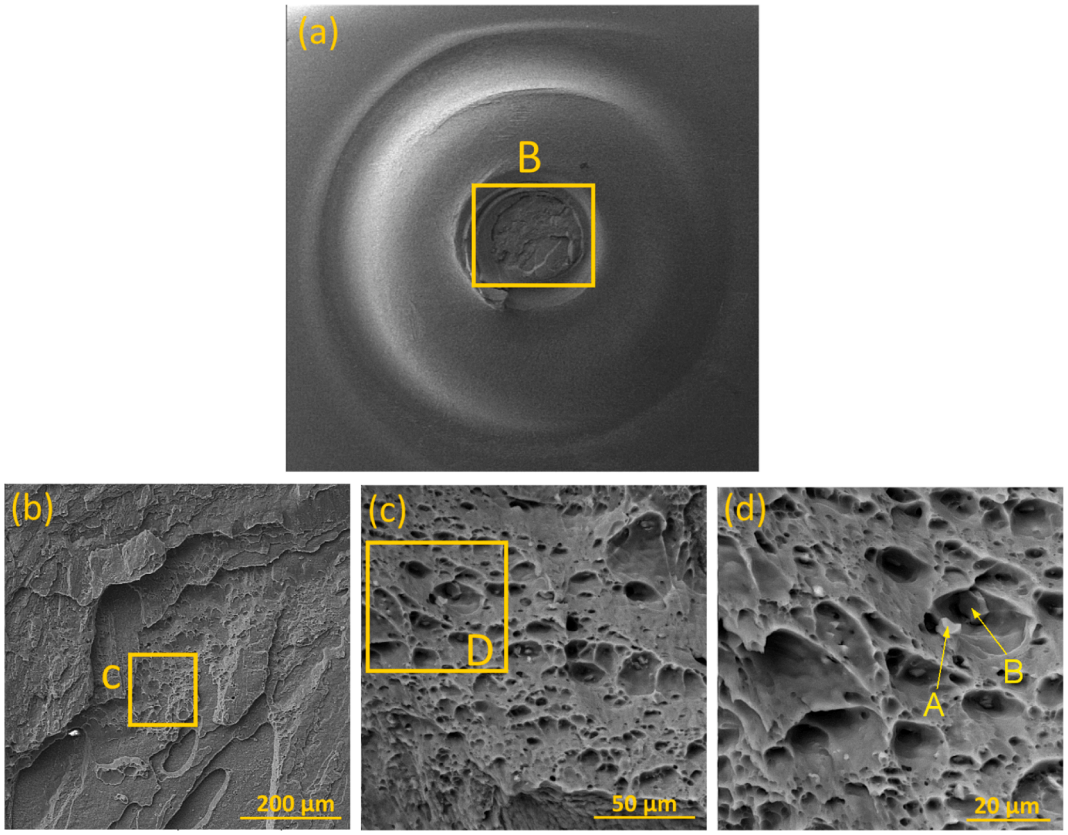

Fig. 27. Fracture SEM-SE images of AA2024-T3/AA5754-O weld (5754 side).

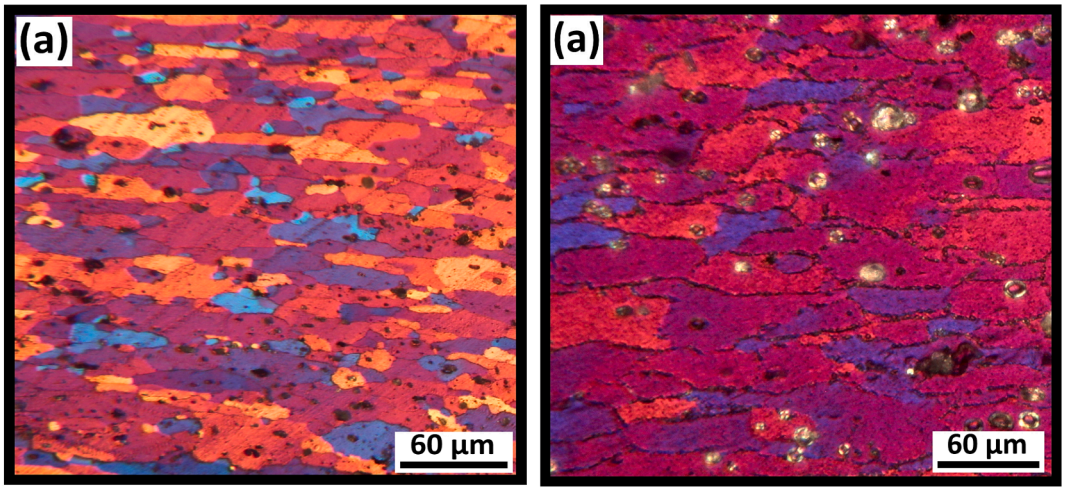

Fig. 28. Microstructure of the base metals (a) AA5754-O and (b) AA2024-T3 alloys.

iii. Material positioning significantly affects peak temperature in both the FSSW and MFSC joints. Higher temperatures are obtained in the joints when harder material is positioned as the upper plate. Maximum temperatures of 500 and 485 °C (MFSC) are attained in the AA2024-T3/AA5754-O and AA5754-O/AA2024-T3 joints respectively while the FSSW counterparts have 475 and 442 °C respectively.

iv. Material positioning induces high dislocation density and tangles in the AA2024-T3/AA5754-O than the AA5754-O/AA2024-T3 joints irrespective of the welding type (MFSC and FSSW).

v. The highest tensile-shear loads of 6317 N and 5366 N are obtained at 1400 rpm in the MFSC welded AA2024-T3/AA5754-O and AA5754-O/AA2024-T3 joints respectively. This occurrence is associated with the disparity between the material flow stresses and the inherent post-weld (in-nugget) dislocation densities.

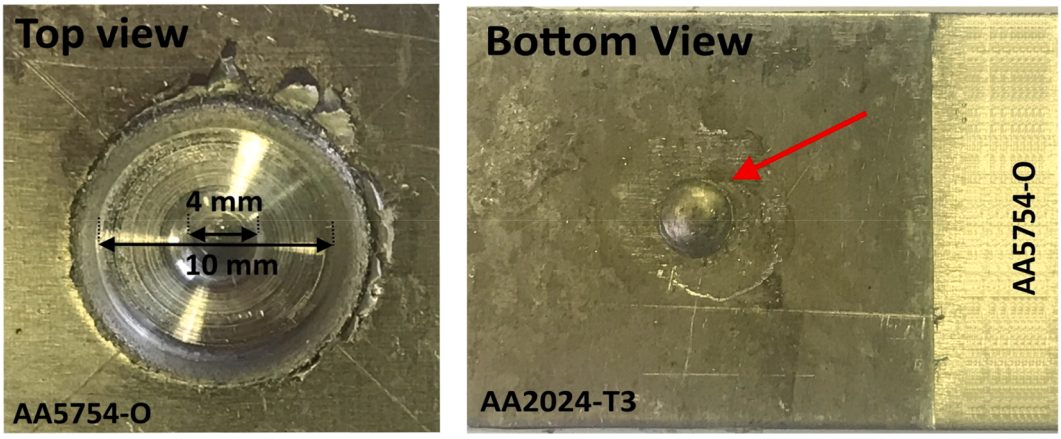

Fig. 29. Joint surface appearance at the 1st stage of the MFSC process (keyhole in the top view, and protrusion in the bottom view).

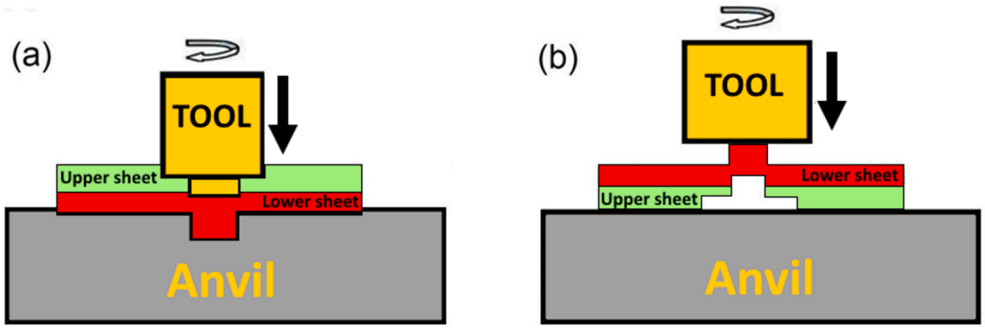

Fig. 30. Schematic illustration of the MFSC process, (a) 1st step, (b) 2nd step.

vi. Material positioning does not affect the fracture mode of the MFSC joint at low rotational speed while it significantly changes the fracture mode at higher tool rotational speed.

Declaration of Competing Interest

The authors declare that they have no known competing financial interests or personal relationships that could have appeared to influence the work reported in this paper.

References

[1] Yuan W, Mishra RS, Webb S, Chen YL, Carlson B, Herling DR, et al. Effect of tool design and process parameters on properties of Al alloy 6016 friction stir spot welds. J Mater Process Technol 2011;211:972–7.
[2] Han Jinzhen, Paidar M, Vaira Vignesh R, Mehta Kush P, Heidarzadeh A, Ojo OO. Effect of shoulder features during friction spot extrusion welding of 2024–T3 to 6061–T6 aluminum alloys. Arch Civil Mech Eng 2020;20. https://doi.org/10.1007/s43452-020-00086-2.
[3] Heidarzadeh A, Mironov S, Kaibyshev R, Çam G, Simar A, Gerlich A, et al. Friction stir welding/processing of metals and alloys: a comprehensive review on microstructural evolution. Prog Mater Sci 2020;100752.
[4] Shen Z, Li WY, Ding Y, Hou W, Liu XC, Guo W, et al. Material flow during refill friction stir spot welded dissimilar Al alloys using a grooved tool. J Manuf Processes 2020;49:260–70.
[5] Shi L, Wu CS, Fu L. Effects of tool shoulder size on the thermal process and material flow behaviors in ultrasonic vibration enhanced friction stir welding. J Manuf Processes 2020;53:69–83.
[6] Mugada Krishna Kishore, Adepu Kumar. Effect of knurling shoulder design with polygonal pins on material flow and mechanical properties during friction stir welding of Al-Mg-Si alloy. Trans Nonferrous Metals Soc China 2019;29. 2281 to 2289.
[7] Sun Z, Wu CS. Influence of tool thread pitch on material flow and thermal process in friction stir welding. J Mater Process Technol 2020;275:116281.
[8] Derazkola HA, Khodabakhshi F, Gerlich AP. Friction-forging tubular additive manufacturing (FFTAM): a new route of solid-state layer-upon layer metal deposition. J Mater Res Technol 2020;9:15273–85.
[9] Derazkola HA, Khodabakhshi F, Gerlich AP. Fabrication of a nanostructured high strength steel tube by friction-forging tubular additive manufacturing (FFTAM) technology. J Manuf Processes 2020;58:724–35.
[10] Paidar M, Ojo O, Moghanian A, Karami Pabandi H, Elsa M. Pre-threaded hole friction stir spot welding of AA2219/PP-C30S sheets. J Mater Process Technol 2019;273:116272.
[11] Memon S, Paidar M, Sadreddini S, Cooke K, Babaei B, Ojo OO. Mechanical and microstructural aspects of the hybrid joint of PP-C30S and 2219 aluminum alloy. Results Phys 2020;19:103629.
[12] Dialami N, Cervera Miguel, Chiumenti Michele. Defect formation and material flow in Friction Stir Welding. Eur J Mech A Solids 2020;80:103912.
[13] Rouzbehani R, Kokabi AH, Sabet H, Paidar M, Ojo OO. Metallurgical, and mechanical properties of underwater friction stir welds of Al7075 aluminum alloy. J Mater Process Technol 2018;262:239–56.
[14] Hakim Ahmad Shah L, Midawi ARH, Walbridge S, Gerlich A. Influence of tool eccentricity on the material flow and microstructural properties of AA6061 aluminum alloy friction stir welds. J Alloy Compd 2020;826:154219.
[15] Mabuwa S, Msomi V. The effect of friction stir processing on the friction stir welded AA1050-H14 and AA6082-T6 joints. Mater Today: Proc 2019. https://doi.org/10.1016/j.matpr.2019.10.039.
[16] Cavaliere P, De Santis A, Panella F, Squillace A. Effect of welding parameters on mechanical and microstructural properties of dissimilar AA6082–AA2024 joints produced by friction stir welding. Mater Des 2009;30:609–16.
[17] Karami Pabandi H, Jashnani HR, Paidar M. Effect of precipitation hardening heat treatment on mechanical and microstructure features of dissimilar friction stir welded AA2024-T6 and AA6061-T6 alloys. J Manuf Processes 2018;31:214–20.
[18] Paidar M, Vaira Vignesh R, Khorram A, Oladimeji Ojo O, Rasoulpouraghdam A, Pustokhina I. Dissimilar modified friction stir clinching of AA2024-AA6061 aluminum alloys: effects of materials positioning. J Mater Res Technol 2020;9:6037–47.
[19] Jeon Chi-Sung, Hong Sung-Tae, Kwon Yong-Jai, Cho Hoon-Hwe, Han Heung Nam. Material properties of friction stir spot welded joints of dissimilar aluminum alloys. Trans Nonferrous Met Soc China 2012;22:605–13.
[20] Paidar M, Ghavamian S, Ojo OO, Khorram A, Shahbaz A. Modified friction stir clinching of dissimilar AA2024-T3 to AA7075-T6: Effect of tool rotational speed and penetration depth. J Manuf Processes 2019;47:157–71.
[21] Paidar M, Ojo OO, Moghanian A, Karapuzha AS, Heidarzadeh A. Modified friction stir clinching with protuberance-keyhole leveling: a process for production of welds with high strength. J Manuf Processes 2019;41:177–87.
[22] Paidar M, Ramalingam VV, Moharrami A, Ojo OO, Jafari A, Sadreddini S. Development and characterization of dissimilar joint between AA2024-T3 and AA6061-T6 by modified friction stir clinching process. Vacuum 2020;176:109298.

[23] Tong L, Xie J, Liu L, Chang G, Ojo OO. Microscopic appraisal and mechanical behavior of hybrid Cu/Al joints fabricated via friction stir spot welding-brazing and modified friction stir clinching-brazing. J Mater Res Technol 2020;9. 13239 to 13249.
[24] Li J, Tang F, Paidar M. Modified friction stir clinching-brazing of brass to AA5083 aluminum alloy using Zn interlayer. Archiv Civ Mech Eng 2021;21:13. https://doi.org/10.1007/s43452-020-00162-7.
[25] Paidar M, Tahani K, Vaira Vignesh R, Oladimeji Ojo O, Ezatpour HR, Moharrami A. Modified friction stir clinching of 2024-T3 to 6061-T6 aluminum alloy: effect of dwell time and precipitation-hardening heat treatment. Mater Sci Eng: A 2020. https://doi.org/10.1016/j.msea.2020.139734.
[26] Memon S, Paidar M, Ojo OO, Cooke K, Babaei B, Masoumnezhad M. The role of stirring time on the metallurgical and mechanical properties during modified friction stir clinching of AA6061-T6 and AA7075-T6 sheets. Results Phys 2020;19:103364.
[27] Zhang G, Xiao C, Ojo OO. Dissimilar friction stir spot welding of AA2024-T3/AA7075-T6 aluminum alloys under different welding parameters and media. Defence Technol 2020. https://doi.org/10.1016/j.dt.2020.03.008.
[28] Ebrahimzadeh V, Paidar M, Safarkhanian MA, Ojo OO. Orbital friction stir lap welding of AA5456-H321/AA5456-O aluminum alloys under varied parameters. Int J Adv Manuf Technol 2018;96:1237–54.
[29] Ojo OO, Taban E, Kaluc E. Friction stir spot welding of aluminum alloys: a recent review. Mater Testing 2015;57:609–27.
[30] Zhang Zhiqiang, He Changshu, Li Ying, Lei Yu, Zhao Su, Zhao Xiang. Effects of ultrasonic-assisted friction stir welding on flow behavior, microstructure and mechanical properties of 7N01-T4 aluminum alloy joints. J Mater Sci Technol 2020;43:1–13.
[31] Li Jianing, Molin Su, Qi Wenjun, Wang Chen, Zhao Peng, Ni Fei, et al. Mechanical property and characterization of 7A04-T6 aluminum alloys bonded by friction stir welding. J Manuf Processes 2020;52:263–9.
[32] Liu Yong, Deng Caiyan, Gong Baoming, Bai Yanan. Effects of heterogeneity and coarse secondary phases on mechanical properties of 7050–T7451 aluminum alloy friction stir welding joint. Mater Sci Eng, A 2019;764:138223.
[33] Zhang HJ, Liu HJ, Song JL, Guan QL, Ji ZJ. Micro-characteristic and formation mechanism of layered band structure in non-weld-thinning friction stir welded 7N01 aluminum alloy. J Manuf Processes 2020;154:154–60.
[34] Zhang Lan, Zhong Huilong, Li Shengci, Zhao Hongjin, Chen Jiqiang, Qi Liang. Microstructure, mechanical properties, and fatigue crack growth behavior of friction stir welded joint of 6061–T6 aluminum alloy. Int J Fatigue 2020;135:105556.
[35] Abbass Muna Khethier, Hussein Sabah Khamass, Khudhair Ahmed Adnan. Optimization of mechanical properties of friction stir spot welded joints for dissimilar aluminum alloys (AA2024-T3 and AA 5754–H114). Arab J Sci Eng 2016;41:4563–72.
[36] Tan YB, Wang XM, Ma M, Zhang JX, Liu WC, Fu RD, et al. A study on microstructure and mechanical properties of AA3003 aluminum alloy joints by underwater friction stir welding. Mater Charact 2017;127:41–52.
[37] Paidar M, Memon S, Samusenkov VO, Babaei B, Ojo OO. Friction spot extrusion welding-brazing of copper to aluminum alloy. Mater Lett 2021;285:129160.
[38] Memon S, Paidar M, Mehta KP, Babaei B, Lankarani HM. Friction spot extrusion welding on dissimilar materials AA2024-T3 to AA5754-O: effect of shoulder plunge depth. J. Mater Eng Perform 2021. https://doi.org/10.1007/s11665-020-05387-4.
[39] Guo Y, Ma Yu'e, Wang Fei. Dynamic fracture properties of 2024–T3 and 7075–T6 aluminum friction stir welded joints with different welding parameters. Theor Appl Fract Mech 2019;104:102372.